bioRxiv preprint doi: https://doi.org/10.1101/2019.12.19.868844; this version posted December 19, 2019. The copyright holder for this preprint (which was not certified by peer review) is the author/funder, who has granted bioRxiv a license to display the preprint in perpetuity. It is made available under aCC-BY-NC-ND 4.0 International license.

Implications of *TP53* Allelic State for Genome Stability, Clinical Presentation and Outcomes in Myelodysplastic Syndromes

Elsa Bernard[1,2], Yasuhito Nannya[3], Robert P. Hasserjian[4], Sean M. Devlin[5], Heinz Tuechler, Juan S. Medina-Martinez[1,2], Tetsuichi Yoshizato[3], Yusuke Shiozawa[3], Ryunosuke Saiki[3], Luca Malcovati[6,7], Max F. Levine[1,2], Juan E. Arango[1,2], Yangyu Zhou[1,2], Francesc Sole[8], Catherine A. Cargo[9], Detlef Haase[10], Maria Creignou[11], Ulrich Germing[12], Yanming Zhang[13], Gunes Gundem[1], Araxe Sarian[2], Arjan A. van de Loosdrecht[14], Martin Jädersten[11], Magnus Tobiasson[11], Olivier Kosmider[15], Matilde Y. Follo[16], Felicitas Thol[17], Ronald F. Pinheiro[18], Valeria Santini[19], Ioannis Kotsianidis[20], Jacqueline Boultwood[21], Fabio P.S. Santos[22], Julie Schanz[10], Senji Kasahara[23], Takayuki Ishikawa[24], Hisashi Tsurumi[25], Akifumi Takaori-Kondo[26], Toru Kiguchi[27], Chantana Polprasert[28], John M. Bennett[29], Virginia M. Klimek[30], Michael R. Savona[31], Monika Belickova[32], Christina Ganster[10], Laura Palomo[8], Guillermo Sanz[33,34], Lionel Ades[35], Matteo Giovanni Della Porta[36], Alexandra G Smith[37], Yesenia Werner[1], Minal Patel[2], Agnès Viale[38], Katelynd Vanness[38], Donna S. Neuberg[39], Kristen E. Stevenson[39], Kamal Menghrajani[30], Kelly L. Bolton[30], Pierre Fenaux[35], Andrea Pellagatti[21], Uwe Platzbecker[40], Michael Heuser[17], Peter Valent[41], Shigeru Chiba[42], Yasushi Miyazaki[43], Carlo Finelli[44], Maria Teresa Voso[45], Lee-Yung Shih[46], Michaela Fontenay[15], Joop H. Jansen[47], José Cervera[48], Yoshiko Atsuta[49], Norbert Gattermann[12], Benjamin L. Ebert[50], Rafael Bejar[51], Peter L. Greenberg[52], Mario Cazzola[6,7], Eva Hellström-Lindberg[11], Seishi Ogawa*[3] and Elli Papaemmanuil*[1,2]

*Shared senior authorship

Affiliations:

[1]Computational Oncology Service, Department of Epidemiology & Biostatistics, Memorial Sloan Kettering Cancer Center, New York, NY, USA.
[2]Center for Hematologic Malignancies, Memorial Sloan Kettering Cancer Center, New York, NY, USA.
[3]Department of Pathology and Tumor Biology, Kyoto University, Kyoto, Japan.
[4]Department of Pathology, Massachusetts General Hospital, Boston, MA, USA.
[5]Department of Epidemiology & Biostatistics, Memorial Sloan Kettering Cancer Center, New York, NY, USA.
[6]Department of Molecular Medicine, University of Pavia, Pavia. Italy.
[7]Department of Hematology, IRCCS Fondazione Policlinico S. Matteo, Pavia. Italy.
[8]MDS Group, Institut de Recerca Contra la Leucèmia Josep Carreras, Barcelona, Spain.
[9]Haematological Malignancy Diagnostic Service, St James's University Hospital, Leeds, United Kingdom.
[10]Clinics of Hematology and Medical Oncology, University Medical Center. Göttingen, Germany.
[11]Department of Medicine Huddinge, Center for Hematology and Regenerative Medicine, Karolinska Institutet, Karolinska University Hospital, Stockholm, Sweden.
[12]Department of Hematology, Oncology and Clinical Immunology, Heinrich Heine University, Düsseldorf, Germany.
[13]Department of Pathology, Memorial Sloan Kettering Cancer Center, New York, NY, USA.
[14]Department of Hematology, VU University Medical Center Amsterdam, The Netherlands.
[15]Department of Hematology, Assistance Publique-Hôpitaux de Paris, Hôpital Cochin and Université de Paris, Université Paris Descartes, Paris, France.
[16]Department of Biomedical and Neuromotor Sciences, University of Bologna, Bologna, Italy.
[17]Department of Hematology, Hemostasis, Oncology and Stem Cell Transplantation, Hannover Medical School, Hannover, Germany.
[18]Drug Research and Development Center, Federal University of Ceara, Ceara, Brazil.

bioRxiv preprint doi: https://doi.org/10.1101/2019.12.19.868844; this version posted December 19, 2019. The copyright holder for this preprint (which was not certified by peer review) is the author/funder, who has granted bioRxiv a license to display the preprint in perpetuity. It is made available under aCC-BY-NC-ND 4.0 International license.

[19]MDS Unit, Hematology, AOU Careggi, University of Florence, Italy.
[20]Department of Hematology, Democritus University of Thrace Medical School, Alexandroupolis, Greece.
[21]Radcliffe Department of Medicine, University of Oxford and Oxford BRC Haematology Theme, Oxford, United Kingdom.
[22]Oncology-Hematology Center, Hospital Israelita Albert Einstein, São Paulo, Brazil.
[23]Department of Hematology, Gifu Municipal Hospital, Gifu, Japan.
[24]Department of Hematology, Kobe City Medical Center General Hospital, Kobe, Japan.
[25]Department of Hematology, Gifu University Graduate School of Medicine, Gifu, Japan.
[26]Department of Hematology and Oncology, Graduate School of Medicine, Kyoto University, Japan.
[27]Department of Hematology, Chugoku Central Hospital, Fukuyama, Japan.
[28]Department of Medicine, Chulalongkorn University, King Chulalongkorn Memorial Hospital, Bangkok, Thailand.
[29]Lab. Medicine and Pathology, Hematology/Oncology, University of Rochester Medical Center, Rochester, NY, USA.
[30]Department of Medicine, Memorial Sloan Kettering Cancer Center, New York, NY, USA.
[31]Department of Medicine, Vanderbilt-Ingram Cancer Center, Vanderbilt University School of Medicine, Nashville, TN, USA.
[32]Department of Genomics, Institute of Hematology and Blood Transfusion, Prague, Czech Republic.
[33]Department of Hematology, Hospital Universitario y Politécnico La Fe, Valencia, Spain.
[34]CIBERONC, Instituto de Salud Carlos III, Madrid, Spain.
[35]Department of Hematology, hôpital St Louis, and Paris University, Paris, France.
[36]Cancer Center, Humanitas Research Hospital & Humanitas University, Milan Italy.
[37]Department of Health Sciences, University of York, United Kingdom.
[38]Integrated Genomics Operation, Memorial Sloan Kettering Cancer Center, New York, NY, USA.
[39]Department of Data Sciences, Dana-Farber Cancer Institute, Boston, MA, USA.
[40]Medical Clinic and Policlinic 1, Hematology and Cellular Therapy, University of Leipzig, Leipzig, Germany.
[41]Department of Internal Medicine I, Division of Hematology and Hemostaseology and Ludwig Boltzmann Institute for Hematology and Oncology, Medical University of Vienna, Austria.
[42]Department of Hematology, Faculty of Medicine, University of Tsukuba, Tsukuba, Japan.
[43]Department of Hematology, Atomic Bomb Disease Institute, Nagasaki University, Japan.
[44]Institute of Hematology, S.Orsola-Malpighi University Hospital, Bologna, Italy.
[45]MDS Cooperative Group GROM-L, Department of Biomedicine and Prevention, Tor Vergata University, Rome, Italy.
[46]Chang Gung Memorial Hospital at Linkou, Chang Gung University, Taiwan.
[47]Laboratory Hematology, Deptartment LABGK, Radboud University Medical Centre, Nijmegen, The Netherlands.
[48]Department of Hematology and Genetics Unit, University Hospital La Fe, Valencia, Spain.
[49]Japanese Data Center for Hematopoietic Cell Transplantation, Nagoya, Japan.
[50]Department of Medical Oncology and Howard Hughes Medical Institute, Dana-Farber Cancer Center, Boston, MA, USA.
[51]UC San Diego Moores Cancer Center, La Jolla, California, USA.
[52]Stanford University Cancer Institute, Stanford, CA, USA.

Address for correspondence: papaemme@mskcc.org

bioRxiv preprint doi: https://doi.org/10.1101/2019.12.19.868844; this version posted December 19, 2019. The copyright holder for this preprint (which was not certified by peer review) is the author/funder, who has granted bioRxiv a license to display the preprint in perpetuity. It is made available under aCC-BY-NC-ND 4.0 International license.

ABSTRACT

TP53 mutations are associated with poor clinical outcomes and treatment resistance in myelodysplastic syndromes. However, the biological and clinical relevance of the underlying mono- or bi-allelic state of the mutations is unclear. We analyzed 3,324 MDS patients for *TP53* mutations and allelic imbalances of the *TP53* locus and found that 1 in 3 *TP53*-mutated patients had mono-allelic targeting of the gene whereas 2 in 3 had multiple hits consistent with bi-allelic targeting. The established associations for *TP53* with complex karyotype, high-risk presentation, poor survival and rapid leukemic transformation were specific to patients with multi-hit state only. *TP53* multi-hit state predicted risk of death and leukemic transformation independently of the Revised International Prognostic Scoring System, while mono-allelic patients did not differ from *TP53* wild-type patients. The separation by allelic state was retained in therapy-related MDS. Findings were validated in a cohort of 1,120 patients. Ascertainment of *TP53* allelic state is critical for diagnosis, risk estimation and prognostication precision in MDS, and future correlative studies of treatment response should consider *TP53* allelic state.

bioRxiv preprint doi: https://doi.org/10.1101/2019.12.19.868844; this version posted December 19, 2019. The copyright holder for this preprint (which was not certified by peer review) is the author/funder, who has granted bioRxiv a license to display the preprint in perpetuity. It is made available under aCC-BY-NC-ND 4.0 International license.

INTRODUCTION

TP53 is the most frequently mutated gene in cancer[1,2]. In patients with myelodysplastic syndromes (MDS), *TP53* mutations have consistently been associated with high-risk disease features such as complex karyotype[3], elevated blasts and severe thrombocytopenia[4]. *TP53*-mutated patients have dismal outcomes[5], rapid transformation[6] to acute myeloid leukemia (AML) and resistance to conventional therapies[7]. Recent studies suggest that *TP53* mutations are predictive of relapse following hematopoietic stem cell transplantation (HSCT)[8,9] and of disease progression during lenalidomide treatment in the context of del(5q)[10]. Upon AML progression, *TP53* mutations demarcate an extremely adverse prognostic group associated with a chemo-refractory disease and less than 2% 5-year survival[11,12]. Therapy-related MDS with *TP53* mutations is similarly associated with dismal outcomes[8,13]. These observations illustrate a central role of *TP53* in the pathogenesis of myeloid neoplasms and highlight its relevance as a prognostic and predictive biomarker. However, *TP53* mutations are not yet considered in clinical risk scores such as the Revised International Prognostic Scoring System (IPSS-R)[14] for MDS.

The majority of *TP53* mutations are missense variants clustering within the DNA binding domain (DBD). Consistent with its role as a tumor suppressor, bi-allelic targeting is mediated by loss of heterozygosity (LOH) involving 17p13 locus, commonly caused by deletion[15]. However, patients present with both mono- and bi-allelic mutations. Functional studies link specific *TP53* mutations with gain of function (GOF) and dominant negative effect (DNE)[16,17,18], which may explain the diverse presentation of *TP53* mutations. Beyond the profound negative effect of *TP53* mutations, the clinical impact of bi-allelic vs. mono-allelic *TP53* mutations on outcomes and response to therapy has not been fully investigated.

We set out to study profiles of genome stability, clinical phenotypes and outcomes of MDS patients with *TP53* mutations in the context of the allelic state. In collaboration with the International Working Group for Prognosis in MDS (IWG-PM) (Supplementary Table. 1), we analyzed a cohort of 3,324 peri-diagnostic and treatment naive patients with MDS or closely related myeloid neoplasms (Extended Data Table 1 and Supplementary Fig. 1). Patient samples were representative of all MDS WHO subtypes and IPSS-R risk groups, and included 563 (17%)

bioRxiv preprint doi: https://doi.org/10.1101/2019.12.19.868844; this version posted December 19, 2019. The copyright holder for this preprint (which was not certified by peer review) is the author/funder, who has granted bioRxiv a license to display the preprint in perpetuity. It is made available under aCC-BY-NC-ND 4.0 International license.

MDS/MPN and 167 (5%) AML/AML with myelodysplasia-related changes (AML-MRC) samples. An additional 1,120 samples derived from the Japanese MDS consortium (Extended Data Table 2) were used as a validation cohort. We described a detailed catalogue of mutagenic processes targeting the *TP53* locus, encompassing acquired mutations, copy-neutral loss of heterozygosity (cnLOH), focal and arm level deletions. We defined distinct *TP53* allelic states and showed that each state is associated with unique profiles of genome stability and clinical presentation. Our findings are of immediate clinical relevance with implications for diagnostic assay development, reporting guidelines and risk stratification of MDS patients.

RESULTS

Characterization of genome wide allelic imbalances in MDS

Genetic profiling included conventional G-banding analyses (CBA) and a custom capture next generation sequencing (NGS) panel that covered *TP53* and genome wide copy-number probes. Allele specific copy-number profiles were generated from NGS data using CNACS[9]. CBA data were available for 2,931 (88%) patients. Comparison of NGS-derived ploidy alterations to CBA-derived ones showed highly concordant results between the two assays (Supplementary Fig. 2 and 3a-b), which allowed us to complement the dataset with NGS findings for 393 cases with missing CBA (Supplementary Fig. 3c). Our custom capture approach further enabled the detection of focal (~3MB) gains or deletions and regions of cnLOH (Supplementary Fig. 4 and Extended Data Fig. 1). Eleven percent of patients (n=360) had at least one cnLOH region, frequently targeting chr17/17p, chr4q, chr7q, chr11q, chr1p and chr14q (Extended Data Fig. 1b). Collectively, 1,571 (47%) patients had one or more chromosomal aberration, of which 329 (10%) had a complex karyotype[19] and 177 (5%) had a monosomal karyotype[20] (Supplementary Table 2).

TP53 mutation landscape in MDS

We identified 486 mutations in *TP53* across 378 individuals. Mutations in *TP53* were annotated as putative oncogenic as previously described[12,21,22] by consideration of 1. Prior evidence in cancer databases[23,24,25]; 2. Recurrence in myeloid disease[5,22,26]; 3. Variant allele frequency (VAF) consistent with somatic representation; 4. Technical controls; and 5. Germline databases[27,28]. The

bioRxiv preprint doi: https://doi.org/10.1101/2019.12.19.868844; this version posted December 19, 2019. The copyright holder for this preprint (which was not certified by peer review) is the author/funder, who has granted bioRxiv a license to display the preprint in perpetuity. It is made available under aCC-BY-NC-ND 4.0 International license.

spectrum of identified *TP53* mutations followed patterns from systematic sequencing studies (Supplementary Fig. 5). As expected, 71% of the mutations were missense variants clustered within the DBD. The 4 most common hotspots (R273, R248, Y220 and R175) accounted for 21% of all mutations.

Among the 378 patients with *TP53* mutations, 274 (72.5%) had a single *TP53* mutation, 100 had two (26.5%) and 4 (1%) had three (Supplementary Fig. 6). We mapped deletions of the *TP53* locus in 97 cases, of which 18 were focal events detected by NGS-based analysis only. We also identified 80 cases with cnLOH which were not detected by CBA (Supplementary Table 3). Approximately half (54%, n=149) of the patients with one *TP53* mutation had loss of the wild-type allele by deletion or cnLOH. In contrast, only 13% (n=14) of patients with ≥2 *TP53* mutations had a concomitant allelic imbalance at the *TP53* locus (OR=8, $p<10^{-13}$ Fisher exact test) (Fig. 1a). According to the number of mutations and the presence of deletion or cnLOH, we defined 4 main *TP53*-mutant subgroups (Fig. 1b): 1. Mono-allelic mutation (n=125, 33% of *TP53*-mutated patients); 2. Multiple mutations without deletion or cnLOH affecting the *TP53* locus (n=90, 24%); 3. Mutation(s) and concomitant deletion (n=85, 22%); 4. Mutation(s) and concomitant cnLOH (n=78, 21%). Additionally, in 24 patients, the *TP53* locus was affected by deletion (n=12), cnLOH (n=2) or isochromosome 17q rearrangement (n=10) without evidence of *TP53* mutations (Fig. 1a).

VAF measurements confirmed that the majority of multi-hit cases were indeed bi-allelic. In patients with ≥2 mutations, the VAFs of mutation pairs were strongly correlated (R^2=0.77, Extended Data Fig. 2a), indicative of bi-allelic state. In 67% (n=60) of those cases, the mutations occurred with certainty in the same cells, with a cumulated VAF exceeding 50% (*the pigeonhole principle*[29]), thus confirming bi-allelic state. In addition, mutations within sequencing read length were systematically observed in trans, i.e., on different alleles (Extended Data Fig. 2b-c). In patients with an allelic imbalance at *TP53*, VAF estimates were enriched for values greater than 50%, consistent with loss of the wild-type allele (Fig. 1c). Taken together, VAF measurements supported bi-allelic targeting of *TP53* on cases with multiple mutations or mutation(s) and allelic imbalances (subgroups 2-4). However, VAF alone was not sufficient to determine allelic state. For example, we identified 19 cnLOH-positive patients with ≤50% *TP53* VAF (median 29%, range

bioRxiv preprint doi: https://doi.org/10.1101/2019.12.19.868844; this version posted December 19, 2019. The copyright holder for this preprint (which was not certified by peer review) is the author/funder, who has granted bioRxiv a license to display the preprint in perpetuity. It is made available under aCC-BY-NC-ND 4.0 International license.

3-49%), suggesting that 24% of cnLOH patients would be misassigned as mono-allelic on the basis of VAF. Therefore, accurate determination of *TP53* allelic state cannot solely rely on *TP53* mutation VAF and should consider LOH mapping, as can be achieved by NGS-based analysis of targeted gene sequencing panels with copy number probes, that are increasingly routine in clinical practice. In mono-allelic cases, VAF densities suggested that *TP53* mutations were enriched for subclonal presentation (median VAF: 13%, median sample purity: 86%) as compared to *TP53* mutations from patients with multiple mutations which were predominantly clonal (median VAF: 32%, median sample purity: 85%) (Fig. 1c).

We organized the *TP53*-mutant subgroups into two states: A. mono-allelic *TP53* state representing subgroup 1, and B. multi-hit *TP53* state encompassing subgroups 2-4, with evidence of at least two *TP53* hits in each patient. While the multi-hit state most likely reflects the presence of clones with bi-allelic targeting, we maintained both "bi-allelic" and "multi-hit" terminology.

Overall, the *TP53* allelic states had shared repertoire of mutations (Fig. 1d and Supplementary Fig. 7). Of note, truncating mutations were enriched in the multi-hit state (28% vs. 14%, OR=2.3, p=0.002 Fisher exact test) while hotspot mutations accounted for 25% of mutations in the mono-allelic state and 20% in the multi-hit state (OR=1.38, p=0.2 Fisher exact test). The differing fractions of hotspot and truncating mutations between states might reflect discrete functional impacts of both mutation types, representing dominant negative vs. simple loss-of-function. In addition, *TP53* allelic state, and by extension whether a wild-type *TP53* allele is retained, points towards differential potential for clonal dominance, whereby the mono-allelic state was confined to smaller sub-clones and the multi-hit state was most frequently clonal.

Implications of *TP53* allelic state to genome stability

The association between *TP53* mutations and chromosomal aneuploidies is well established[3,9,11,12]. Overall, 67% (n=252) of *TP53*-mutated cases had ≥2 chromosomal deletions as compared to 5% (n=158) of wild-type cases (OR=35, $p<10^{-16}$ Fisher exact test). Excluding chr17 (which is linked to state definition), there was a significantly higher number of chromosomal aberrations per patient, across rearrangements, gains and deletions, in all *TP53* subgroups of

bioRxiv preprint doi: https://doi.org/10.1101/2019.12.19.868844; this version posted December 19, 2019. The copyright holder for this preprint (which was not certified by peer review) is the author/funder, who has granted bioRxiv a license to display the preprint in perpetuity. It is made available under aCC-BY-NC-ND 4.0 International license.

multiple hits compared to the mono-allelic state (Fig. 2a and Extended Data Fig. 3). This enrichment was most pronounced for deletions (median 4 in multi-hit vs. 1 in mono-allelic state, $p<10^{-16}$ Wilcoxon rank-sum test, Fig. 2a). In particular, deletion of 5q was observed in 85% of multi-hit patients as opposed to 34% of mono-allelic patients (OR=10, $p<10^{-16}$ Fisher exact test, Supplementary Fig. 8). Taken together, we found a median of 6 unique chromosomal aberration in the multi-hit state and 1 in the mono-allelic state ($p<10^{-16}$ Wilcoxon rank-sum test, Fig. 2b). Our data suggest that residual wild-type *TP53* is critical to maintenance of genome stability, and that the association between *TP53* and complex karyotype is specific to the multi-hit state (91% vs. 13% complex karyotype patients within multi-hit or mono-allelic states, OR=70, $p<10^{-16}$ Fisher exact test, Fig. 2c).

TP53 allelic state associates with distinct clinical phenotype and shapes patient outcomes

Without discriminating allelic states, previous studies uniformly reported adverse effects of *TP53* mutations on clinical phenotypes and outcome[3,4]. These were recapitulated in our study (Supplementary Fig. 9 and 10). However, when analyzed separately, the two *TP53* allelic states associated with distinct clinical presentation and outcomes.

Mono-allelic *TP53* patients were less cytopenic (Fig. 3a-c) and had lower percentages of bone marrow blasts compared to multi-hit patients (median 4 vs. 9%, $p<10^{-10}$ Wilcoxon rank sum test, Fig. 3d). There was a higher prevalence of lower risk MDS subtypes such as isolated del(5q) in mono-allelic patients, while the multi-hit state was enriched for higher risk WHO subtypes (Extended Data Fig. 4a). In IPSS-R, 46% of the mono-allelic *TP53* cases classified as good/very-good and 29% as poor/very-poor risk, whereas only 5.5% of multi-hit cases stratified as good/very-good and 89% as poor/very-poor risk (Extended Data Fig. 4b). These observations link *TP53* allelic state to disease presentation, WHO and IPSS-R risk classifications, whereby multi-hit state was enriched in higher risk disease.

The two allelic states had very different effects on overall survival (OS) and AML transformation. The median OS in mono-allelic *TP53* state was 2.5 years (95% CI: 2.2-4.9 years) and 8.7 months in the multi-hit state (95% CI: 7.7-10.3 months) (HR=3.7, 95% CI: 2.7-5.0, $p<10^{-16}$ Wald test). In comparison, wild-type patients had a median OS of 3.5 years (95% CI: 3.4-3.9 years) (Fig. 4a).

bioRxiv preprint doi: https://doi.org/10.1101/2019.12.19.868844; this version posted December 19, 2019. The copyright holder for this preprint (which was not certified by peer review) is the author/funder, who has granted bioRxiv a license to display the preprint in perpetuity. It is made available under aCC-BY-NC-ND 4.0 International license.

The effect of mono-allelic *TP53* on OS was independent and not confounded by del(5q) (Supplementary Fig. 11). The 5-year cumulative incidence of AML transformation in mono-allelic *TP53* was 21% and 44% in the multi-hit state (HR=5.5, 95% CI: 3.1-9.6, $p<10^{-8}$ Wald test) (Fig. 4b). Of note, the different *TP53*-subgroups defining the multi-hit state (multiple mutations, mutation(s) and deletion or cnLOH) had equally dismal outcomes (Extended Data Fig. 5), illustrating that the various mutagenic processes leading to bi-allelic targeting of *TP53* equally shape the clinical routes of MDS patients.

The OS separation of the two *TP53* states transcended disease subtypes and was significant across most WHO classes (Extended Data Fig. 6a). It was less pronounced in MDS with excess blasts and AML/AML-MRC arguably because other dominant risk factors exist besides *TP53* allelic state. Differences in outcomes between *TP53* states were also independent of IPSS-R risk groups (Extended Data Fig. 6b), and multi-hit *TP53* state identified patients with poor survival across IPSS-R strata. Notably, 10% of multi-hit patients were classified as IPSS-R good/very-good or intermediate risk. The implication of this finding is that assessment of *TP53* allelic state is critical to identify higher risk patients. In fact, multivariable Cox proportional hazards models that included *TP53* state alongside age of diagnosis, cytogenetic risk score[19] and established predictive features identified multi-hit *TP53* as an independent predictor for the risk of death and AML transformation (HR_{OS}=2.04, 95% CI: 1.6-2.6, $p<10^{-7}$; HR_{AML}=2.9, 95% CI: 1.8-4.7, $p<10^{-5}$ Wald test), whereas mono-allelic *TP53* state did not influence OS or AML transformation compared to wild-type *TP53* (Fig. 4c-d). The same conclusion resulted from multivariable models that considered overall IPSS-R score (Supplementary Fig. 12).

Recent studies reported additive risk effects for *TP53* mutations and complex karyotype[3,11,12], highlighting that each independently contribute to a patient risk. In multivariable analyses, multi-hit *TP53* state and complex karyotype, but not mono-allelic *TP53*, were independent predictors of adverse outcome (Supplementary Fig. 13). Despite the strong correlation between multi-hit *TP53* and complex karyotype, the additive risk effects remained in this setting, whereby patients with complex karyotype and multi-hit *TP53* state did worse than patients with either complex or multi-hit *TP53* (Supplementary Fig. 13b-c). In the absence of complex karyotype, mono-allelic *TP53* patients had similar survival than wild type patients while multi-hit *TP53*

bioRxiv preprint doi: https://doi.org/10.1101/2019.12.19.868844; this version posted December 19, 2019. The copyright holder for this preprint (which was not certified by peer review) is the author/funder, who has granted bioRxiv a license to display the preprint in perpetuity. It is made available under aCC-BY-NC-ND 4.0 International license.

patients had an increased risk of death (Supplementary Fig. 13c). This emphasizes the importance of mapping *TP53* state alongside complex karyotype for accurate risk estimation.

TP53 mutation VAF had been reported to be of prognostic significance in MDS[30]. This is likely explained by the strong correlation between high VAF, especially for values exceeding 50%, and bi-allelic targeting. However, we showed that VAF as a criterion cannot accurately capture the entire spectrum of patients with bi-allelic targeting, which includes patients with more than one *TP53* mutations in the absence of allelic imbalance and patients with subclonal cnLOH at VAF ≤50% (Fig. 1b-c and Extended Data Fig. 2). Optimal cut-point analysis[31] identified that patients with mono-allelic *TP53* mutations and VAF>23% (n=34) had increased risk of death compared to wild-type patients (HR=2.2, 95% CI: 1.5-3.2, $p<10^{-3}$ Wald test), whereas patients with mono-allelic *TP53* mutations and VAF≤23% (n=91) had similar OS than wild-type patients (Supplementary Fig. 14). While we may have missed a second *TP53* hit in the small subset of mono-allelic cases with VAF>23%, this shows that patients with mono-allelic mutations and high VAF should be closely monitored. Conversely, multi-hit patients had poor outcomes across all ranges of VAF, whereby even the subset of patients with low VAF≤10% (n=20) had very dismal outcome (Supplementary Fig. 14). This highlights that VAF alone is not sufficient to determine *TP53* allelic state, which requires assessment of both mutations and allelic imbalances, and that multi-hit *TP53* state identifies very high-risk patients independently of the VAF of *TP53* mutations.

Effect of *TP53* mutation types in clinical outcomes

The emergence of data in support of DNE[18,32] and GOF[33,34,35] led us to test whether outcomes differed based on the nature of the underlying lesion, i.e., missense, truncated or hotspot mutations. In the multi-hit state, no differences were observed on genome instability levels (Extended Data Fig. 7) and outcomes (Extended Data Fig. 7 and Supplementary Fig. 15a-b) across mutation types, showcasing that it is the loss of both wild-type copies of *TP53* that drive the dismal outcomes of *TP53*-mutated MDS patients rather than the underlying mutation types.

In the mono-allelic state, missense mutations in the DBD as a whole had no effect on patient outcomes compared to wild-type *TP53*. However, there was an increased risk of death of

bioRxiv preprint doi: https://doi.org/10.1101/2019.12.19.868844; this version posted December 19, 2019. The copyright holder for this preprint (which was not certified by peer review) is the author/funder, who has granted bioRxiv a license to display the preprint in perpetuity. It is made available under aCC-BY-NC-ND 4.0 International license.

mono-allelic *TP53* patients with hotspot mutations (R175, R248) compared to wild-type patients (HR=1.7, 95% CI: 1.1-2.8, p=0.02 Wald test, Supplementary Fig. 15c-d). This is consistent with either DNE or GOF of the hotspot mutant proteins with increased selection of these mutated residues. But this observation was not uniform across all mono-allelic missense mutations, suggesting that the putative DNE[18] may not be equivalent across DBD mutations. Definitive conclusions on the possible non-equivalence of mono-allelic missense mutations warrant evaluation in larger datasets and functional studies that extend beyond the mutation hotspots.

Consequences of *TP53* allelic state in therapy-related MDS

Our cohort included 229 cases with therapy-related MDS (t-MDS), which were enriched[8,13] for *TP53*-mutated patients relative to de-novo MDS (18% vs. 6%, OR=3.3, $p<10^{-11}$ Fisher exact test). The *TP53*-mutated t-MDS patients had a higher proportion of multiple hits compared to *TP53*-mutated de-novo patients (84% vs. 65%, OR=2.8, p=0.002 Fisher exact test). Comparison of genome profiles (Supplementary Fig. 16) and clinical outcomes (Fig. 5a) between *TP53* allelic states reiterated observations in de-novo MDS. *TP53*-mutant t-MDS is considered one of the most lethal malignancies with limited treatment options[7], yet mono-allelic *TP53* had lower risk of death compared to multi-hit *TP53* even in the t-MDS setting (HR=0.39, 95% CI: 0.15-1.0, p=0.05 Wald test).

TP53 allelic state and disease progression

We analyzed serial data from 12 MDS patients of an independent cohort collected from the diagnostic service of St James's University Hospital (Leeds, United Kingdom)[36,37] who progressed to AML with a *TP53* mutation in either disease phase (Supplementary Fig. 17). We found a preponderance of two *TP53* hits at the time of MDS diagnosis (7/12 cases, with a median of 4 months to AML progression) (Supplementary Fig. 17a-g). In 3 patients, bi-allelic targeting occurred during disease progression with evidence of inter-clonal competition and attainment of clonal dominance for the *TP53* clone (Supplementary Fig. 17h-i). The remaining two cases that progressed with a mono-allelic *TP53* mutation had other high-risk mutations in *RUNX1* and *KRAS* or in *CBL* (Supplementary Fig. 17k-l). These data provided further evidence that bi-allelic

bioRxiv preprint doi: https://doi.org/10.1101/2019.12.19.868844; this version posted December 19, 2019. The copyright holder for this preprint (which was not certified by peer review) is the author/funder, who has granted bioRxiv a license to display the preprint in perpetuity. It is made available under aCC-BY-NC-ND 4.0 International license.

alteration of *TP53* is a potent driver of disease progression and underscored the importance of assessing *TP53* allelic state at diagnosis and for disease surveillance.

Validation cohort

We tested our findings in 1,120 MDS patients with comparable molecular annotations. We validated the representation of *TP53* allelic states (Supplementary Fig. S18), genome stability profiles (Supplementary Fig. S19) and differences in clinical phenotypes (Supplementary Fig. S20). Our validation cohort was enriched for higher risk disease subtypes compared to our study cohort (Extended Data Table 1 and 2). Overall, multi-hit patients had significantly increased risk of death than mono-allelic patients (Supplementary Fig. S20e). Within lower-risk disease subgroups, OS of mono-allelic *TP53* patients was similar to that of wild-type patients (Supplementary Fig. S20f).

TP53 allelic state on treatment response

Recent studies report poor responses to lenalidomide[10] and HSCT[8,9] for *TP53*-mutated patients, and marked but transient response to HMA[38]. We conducted an exploratory analysis of overall survival per *TP53* state of patients that received hypomethylating agent (HMA) (Fig. 5b), lenalidomide on the subset with del(5q) (Fig. 5c) and following HSCT (Fig. 5d). On HMA and lenalidomide, patients with mono-allelic *TP53* mutations had evidence of longer survival compared to multi-hit patients (Fig. 5b-c). The analysis of our HSCT cohort was limited due to its size, yet we observed a trend for improved survival of mono-allelic patients compared to multi-hit patients following HSCT (Fig. 5d). These observations highlight the importance of mapping allelic state in future correlative studies of *TP53* response to therapy.

DISCUSSION

The increasing prevalence of molecular profiling in clinical practice calls for an improved mapping of genotype features to clinical outcomes, in order to identify meaningful biomarkers and institute precision medicine practices[39]. Beyond biomarker validation, the delivery of precision medicine practices is increasingly reliant upon precision diagnostics. This study

bioRxiv preprint doi: https://doi.org/10.1101/2019.12.19.868844; this version posted December 19, 2019. The copyright holder for this preprint (which was not certified by peer review) is the author/funder, who has granted bioRxiv a license to display the preprint in perpetuity. It is made available under aCC-BY-NC-ND 4.0 International license.

unraveled the distinct effects of the allelic states of *TP53*, the most frequently mutated gene in cancer[1,2], with clinical implications for diagnosis, disease surveillance and risk stratification.

We developed a novel framework for the ascertainment of *TP53* mutations, focal deletions and cnLOH from unmatched custom capture sequencing data. Our copy-number tools CNACS is accessible from an open-source software development platform (https://github.com/papaemmelab/toil_cnacs). Through integrative analyses of the mutagenic processes targeting *TP53*, coupled with large sample size and robust clinical annotation, we were able to accurately characterize *TP53* allelic states and evaluate their clinical implications in MDS.

TP53 is universally considered as an adverse prognostic biomarker associated with genome instability, treatment resistance, disease progression and dismal outcomes[16,40]. We provided strong and definitive evidence that the multi-hit *TP53* state in MDS, not the bare presence of any *TP53* mutation, underlies these associations. It is therefore critical to accurately assess *TP53* allelic state in the diagnostic workup of MDS patients. Combining information from the number of *TP53* mutations, CBA, VAF and LOH status derived from NGS-based copy-number analysis or SNP arrays would allow clinical laboratories to discriminate between the vast majority of bi-allelic and mono-allelic *TP53* mutations. Fig. 6 suggests an easily implementable workflow for the assessment of *TP53* allelic state in routine clinical practice. We propose that bi-allelic *TP53* state should be distinguished from mono-allelic *TP53* mutations in future revisions of the IPSS-R and correlative studies of treatment response. This is meaningful for clinical practice as one in three *TP53*-mutated patients is mono-allelic. In our cohort, mono-allelic patients did not differ from *TP53* wild-type patients with regards to genome stability, response to therapy, overall survival and progression to AML. Although *TP53* is the most scrutinized cancer gene, our study materializes to our knowledge the first assessment of the impact of the allelic state of *TP53* on disease biology and clinical outcomes in large MDS patient cohorts. Given the importance of *TP53* in cancer, these findings warrant further investigation across cancer indications.

bioRxiv preprint doi: https://doi.org/10.1101/2019.12.19.868844; this version posted December 19, 2019. The copyright holder for this preprint (which was not certified by peer review) is the author/funder, who has granted bioRxiv a license to display the preprint in perpetuity. It is made available under aCC-BY-NC-ND 4.0 International license.

METHODS

Patient samples

The IWG-PM cohort originated from 24 MDS centers (Supplementary Table 1) that contributed peri-diagnosis MDS, MDS/MPN and AML/AML-MRC patient samples to the study. Upon quality control (Supplementary Fig. 1), 3,324 samples were included in the study (Extended Data Table 1). The source for genomic DNA was bone marrow or peripheral blood. The median time from diagnosis to sampling was 0 days (1st quartile: 0 days, 3rd quartile: 113 days). The validation cohort consisted of 1,120 samples from the Japanese MDS consortium (Extended Data Table 2). Samples were obtained with informed consent in accordance with the Declaration of Helsinki and appropriate Ethics Committee approvals.

Clinical data

Diagnostic clinical variables were provided by the contributing centers and curated to ensure uniformity of metrics across centers and countries. Clinical variables included i) Sex ii) Age at diagnosis iii) WHO disease subtype iv) MDS type i.e., de-novo, secondary or therapy-related MDS v) Differential blood counts to include hemoglobin, platelets, white blood cell, neutrophil and monocyte vi) Percentage of bone marrow and peripheral blood blasts vii) Cytogenetic data and viii) Risk score as per the IPSS-R[14]. Clinical outcomes included the time of death from any cause or last follow-up from sample collection, and the time of AML transformation or last follow-up from sample collection. Detailed cohort characteristics are provided in Extended Data Table 1 and 2.

Cytogenetic data

CBA data were available for 2,931 patients and karyotypes were described in accordance to the International System for Human Cytogenetic Nomenclature[41]. CBA data were risk stratified according to the IPSS-R guidelines[19] using both algorithmic classification and manual classification by an expert panel of cytogeneticists.

bioRxiv preprint doi: https://doi.org/10.1101/2019.12.19.868844; this version posted December 19, 2019. The copyright holder for this preprint (which was not certified by peer review) is the author/funder, who has granted bioRxiv a license to display the preprint in perpetuity. It is made available under aCC-BY-NC-ND 4.0 International license.

WHO subtypes

Contributing centers provided for the vast majority disease classification as per WHO 2008. Pathology review was performed uniformly on the entire cohort, to ensure concordance between disease classification and diagnostic variables, and to update the classification as per WHO 2016.

IPSS-R risk scores

IPSS-R risk scores were uniformly calculated based on the IPSS-R cytogenetic risk scores and on the values for hemoglobin, platelets, absolute neutrophil count and percentage of bone marrow blasts.

Targeted sequencing

Panel design

The panel used for targeted sequencing included 1,118 genome wide single nucleotide polymorphism (SNP) probes for copy number analysis, with on average one SNP probe every 3Mb. Bait tiling was conducted at 2x. Baits were designed to span all exonic regions of *TP53* across all transcripts, as described in RefSeq (NM_001276761, NM_001276695, NM_001126114, NM_00112611), and included 20bp intronic flanking regions.

Library preparation and sequencing

For library construction, 11-800ng of genomic DNA was used using the KAPA Hyper Prep Kit (Kapa Biosystems KK8504) with 7-12 cycles of PCR. After sample barcoding, 10-1610ng of each library were pooled and captured by hybridization. Captured pools were sequenced with paired-end Illumina HiSeq at a median coverage of 730x per sample (range 127-2480x). Read length was 100bp or 125bp.

We also sequenced 48 samples on the panel, with the same sequencing conditions as the tumor samples, from young individuals who did not have hematological disease; to help further filtering of sequencing artefacts and germline SNPs.

bioRxiv preprint doi: https://doi.org/10.1101/2019.12.19.868844; this version posted December 19, 2019. The copyright holder for this preprint (which was not certified by peer review) is the author/funder, who has granted bioRxiv a license to display the preprint in perpetuity. It is made available under aCC-BY-NC-ND 4.0 International license.

Sequencing was performed in an unmatched setting i.e., without a matched normal tissue control per patient, so that variants had to be curated accordingly (see section "*TP53* variant annotation" below).

Alignment

Raw sequence data were aligned to the human genome (NCBI build 37) using BWA[42] version 0.7.17. PCR duplicate reads were marked with Picard tools (https://broadinstitute.github.io/picard/) version 2.18.2. For alignment, we used the pcap-core dockerized pipeline version 4.2.1 available at https://github.com/cancerit/PCAP-core/wiki/Scripts-Reference-implementations.

Sample quality control

Quality control (QC) of the fastq data and bam data were performed with FastQC (http://www.bioinformatics.babraham.ac.uk/projects/fastqc/) version 0.11.5 and Picard tools respectively.

In addition, a number of downstream QC steps were performed, to include:

- Fingerprinting, i.e., evaluation of the similarity between all pairs of samples based on the respective genotype on 1,118 SNPs. Duplicate samples were excluded from the study.
- Evaluation of concordance between the patient sex from the clinical data and the coverage on the sex chromosomes. Discordant cases were discussed with the contributed centers to rule out patients with Klinefelter syndrome and filter out erroneous samples appropriately.
- Evaluation of concordance between CBA data and NGS derived copy-number profiles (see section "Copy number analysis" below). A typical discordant case is a case where CBA reports a given deletion or gain in a high number of metaphases and NGS profile clearly shows other abnormalities but not the one reported by CBA. All discordant cases were reviewed by a panel of experts through the IWG cytogenetic committee.

bioRxiv preprint doi: https://doi.org/10.1101/2019.12.19.868844; this version posted December 19, 2019. The copyright holder for this preprint (which was not certified by peer review) is the author/funder, who has granted bioRxiv a license to display the preprint in perpetuity. It is made available under aCC-BY-NC-ND 4.0 International license.

Finally, samples that passed QC but were found not to be treatment naive i.e., the patients received disease modifying treatment before sample collection were excluded from the study. Supplementary Fig. 1 summarizes the QC workflow.

TP53 variant calling

Variants in *TP53* were called using a combination of variant callers. For single nucleotide variants (SNVs), we used Caveman (http://cancerit.github.io/CaVEMan/) version 1.7.4, Mutect[43] version 4.0.1.2 and Strelka[44] version 2.9.1. For small insertions and deletions, we used Pindel[45] version 1.5.4, Mutect version 4.0.1.2 and Strelka version 2.9.1. VAFs were uniformly reported across all called variants using a realignment procedure (https://github.com/cancerit/vafCorrect).

Likely artefact variants were filtered out based on:

- The number of callers calling a given variant and the combination of filters from the triple callers.
- Variants with VAF<2%, less than 20 total reads or less than 5 mutant supporting reads were excluded.
- Recurrence and VAF distribution of the called variants on a panel of normals.
- Off-target variants, i.e., variants called outside of the panel target regions were not considered.

TP53 variant annotation

All called variants were annotated with VAGrENT (https://github.com/cancerit/VAGrENT) version 3.3.0 and Ensembl-VEP (https://github.com/Ensembl/ensembl-vep) with Ensembl version 91 and VEP release 94.5.

After pre-filtering of artifactual variants, likely germline SNPs were filtered out by consideration of:

- VAF density of variants consistent with germline SNP.
- Presence in the Genome Aggregation Database (gnomAD)[46].

bioRxiv preprint doi: https://doi.org/10.1101/2019.12.19.868844; this version posted December 19, 2019. The copyright holder for this preprint (which was not certified by peer review) is the author/funder, who has granted bioRxiv a license to display the preprint in perpetuity. It is made available under aCC-BY-NC-ND 4.0 International license.

- Recurrence in panel of normals.

All remaining likely somatic *TP53* variants were manually inspected with the Integrative Genomics Viewer (IGV)[47] to rule out residual artefacts.

From the list of likely somatic *TP53* variants, putative oncogenic variants were distinguished from variants of unknown significance (VUS) based on:

- The inferred consequence of a mutation; where nonsense and splice SNVs, and frameshift insertions and deletions were considered oncogenic.
- Recurrence in the Catalogue Of Somatic Mutations in Cancer (COSMIC)[24], in myeloid disease samples registered in cBioPortal[24,48] or in the study dataset.
- Presence in pan-cancer hotspot analysis as described in[49] and[50].
- Annotation in the human variation database ClinVar[28].
- Annotation in the precision oncology knowledge database OncoKB[23].
- Functional annotation in the International Agency for Research on Cancer (IARC) *TP53* database[25].
- *TP53* functional classification prediction scores using PHANTM[51].
- Recurrence with somatic presentation in a set of in-house data derived from >6,000 myeloid neoplasms[12,21,22].

Copy number analysis

We assessed chromosomal alterations based on NGS sequencing data using CNACS[9]. CNACS enables the detection of arm level and focal copy-numbers changes as well as regions of cnLOH. CNACS has been optimized to run in the unmatch setting and uses a panel of normals for calibration. CNACS[9] is available as a python toil workflow engine at https://github.com/papaemmelab/toil_cnacs, where release v0.2.0 was used in this study.

Supplementary Fig. 2 provides examples of characterization of allelic imbalances (gains, deletions and regions of cnLOH) using CNACS, with concordant copy-number change findings between CBA and CNACS, focal deletions exclusively detected with CNACS and, as expected, regions of cnLOH exclusively detected by CNACS. Supplementary Fig 3a-b provides a

bioRxiv preprint doi: https://doi.org/10.1101/2019.12.19.868844; this version posted December 19, 2019. The copyright holder for this preprint (which was not certified by peer review) is the author/funder, who has granted bioRxiv a license to display the preprint in perpetuity. It is made available under aCC-BY-NC-ND 4.0 International license.

genome-wide characterization of allelic imbalances on 2,931 MDS patients and compares the levels of detection from CBA and CNACS. Note that for genome-wide analysis, we restricted the CNACS gain, deletion or cnLOH segments to be bigger than 3Mb. Supplementary Fig 4 provides examples of characterization of allelic imbalances by CNACS and SNP arrays on 21 selected samples, with extremely concordant findings between the two assays.

In addition to CNACS, we also run CNVkit[52] version 0.9.6 on the study cohort. CNVkit does not infer allele specific copy-numbers, so that it does not allow to mark regions of cnLOH, but it estimates copy-number changes. The integration of two copy-number tools allowed to increase specificity and sensitivity of the calling.

On 2,931 patients with CBA data, we performed a detailed comparison of CBA and CNACS results (Supplementary Fig. 3). Along the annotation of regions of cnLOH, we supplemented the presence of copy-number changes on those patients when it was clear on the NGS results but missed by CBA. For the 393 patients with missing CBA data, we used the NGS results to annotate copy-number changes. As our NGS assay did not allow to detect translocations, inversions, whole genome amplification and the presence of marker or ring chromosomes, those specific alterations were statistically imputed from other molecular markers on the 393 patients with missing CBA.

Complex Karyotype

From the 2,931 patients with CBA data, 310 had a complex karyotype according to the CBA results, where complex karyotype was defined as 3 or more independent chromosomal abnormalities. Within the 2,931 patients with CBA data, CNACS results helped to identify complex karyotype in an additional 15 patients. Within the 393 cases with missing CBA data, 13 had a complex karyotype according to NGS copy-number profiles (Supplementary Fig. 3c). Overall, 329 patients had complex karyotype representing 10% of the study cohort.

Survival analysis

All statistical analyses were conducted using the R statistical platform (R Core Team 2019) (https://www.r-project.org/).

bioRxiv preprint doi: https://doi.org/10.1101/2019.12.19.868844; this version posted December 19, 2019. The copyright holder for this preprint (which was not certified by peer review) is the author/funder, who has granted bioRxiv a license to display the preprint in perpetuity. It is made available under aCC-BY-NC-ND 4.0 International license.

Overall survival

OS was measured from the time of sample collection to the time of death from any cause. Patients alive at the last follow-up date were censored at that time. Survival probabilities over time were estimated using Kaplan-Meier methodology, and comparisons of survival across *TP53*-mutant subgroups were conducted using the logrank test.

Multivariable models of OS were performed with Cox proportional hazards regressions. Hazard ratios and 95% confidence intervals were reported for the covariates along the p-values from the Wald test. Covariates included in the multivariable model of OS shown in Fig. 3c were age, hemoglobin, platelets, absolute neutrophil count (ANC), bone marrow blasts, cytogenetic risk group and *TP53* allelic state. Hemoglobin, platelets, ANC and bone marrow blasts were treated as continuous variables and were scaled by their sample mean. Age was treated as a continuous variable and was scaled by a factor 10. Cytogenetic risk group was treated as a categorical variable with the intermediate risk group as the reference group. *TP53* allelic state was treated as a categorical variable with the wild-type state as the reference group relative to the mono-allelic and the multi-hit groups. Note that those covariates correspond to all covariates included in the age-adjusted IPPS-R model in addition to *TP53* allelic state.

AML transformation

In univariate analysis of AML transformation (AMLt), time to AMLt was measured from the time of sample collection to the time of transformation, with death without transformation treated as a competing risk. Patients alive without AMLt at the last contact date were censored at that time. Cumulative incidence functions were used to estimate the incidence of AMLt and comparisons of cumulative incidence function across *TP53*-mutant subgroups were conducted using the Gray's test.

Multivariable models of AMLt were performed using cause-specific Cox proportional hazards regressions, where patients who did not transform but died were censored at the time of death. Hazard ratios and 95% confidence intervals were reported for the covariates along the p-values

bioRxiv preprint doi: https://doi.org/10.1101/2019.12.19.868844; this version posted December 19, 2019. The copyright holder for this preprint (which was not certified by peer review) is the author/funder, who has granted bioRxiv a license to display the preprint in perpetuity. It is made available under aCC-BY-NC-ND 4.0 International license.

from the Wald test. Covariates included in the multivariable model of AMLt shown in Fig. 3d were the same as the ones included in the model of OS described above.

AUTHOR CONTRIBUTIONS

E.B. and E.P. designed the study. E.B., Y.N. and T.Y. performed statistical analysis. S.D. and E.P. supervised statistical analysis. L.M., B.L.E, R.B., P.L.G., M. Cazzola, E.H-L., S.O. and E.P. supervised research. P.L.G. and E.P. coordinated the study. L.M., F.S., C.A.C., M. Creignou, U.G., A.A.L., M.J., M.T., O.K., M.Y.F., F.T., R.F.P., V.S., I.K., J.B., F.P.S.S., S.K., T.I., T.H., A.K.T., T.K., C.P., V.M.K., M.R.S., M.B., C.G., L.P., L.A., M.G.D.P., P.F., A.P., U.P., M.H., P.V., S.C., Y.M., C.F., M.T.V., L-Y.S., M.F., J.H.J., J.C., Y.A., N.G., M. Cazzola, E.H-L. and S.O. provided clinical data and DNA specimens. E.B., Y.W., M.P. and E.P. coordinated sample acquisition. A.V. and K.V. performed sample preparation and sequencing. E.B., R.P.H., H.T. and M. Creignou curated clinical data. R.P.H. and J.M.B. performed pathology review. E.B. and H.T. processed cytogenetic data. F.S., D.H. and J.S. performed cytogenetic review. E.B., Y.N., J.S.M-M, T.Y., A.S. and G.G. performed bioinformatic analysis. J.S.M-M, M.F.L., J.E.A. and J.Z. supported sequence data pipelines. Y.S. and R.S. developed copy-number algorithm CNACS. M.F.L. generated copy-number profiles. Y.Z. performed SNP array analysis. E.B. and Y.N. prepared figures and tables. E.B., S.O. and E.P. wrote the manuscript. All authors reviewed the manuscript during its preparation.

ACKNOWLEDGEMENTS

Supported in part by grants from Celgene Corporation through and MDS Foundation, Inc, Yardville, NJ; J.B. and A.P. acknowledge funding from Bloodwise grant 13042; P.V. was supported by the Austrian Science Fund (FWF) grant F4704-B20; M.Y. F. was supported by Italian MIUR-PRIN grants; L.M. was supported by the Associazione Italiana per la Ricerca sul Cancro (AIRC, Milan, Italy) 5×1000 project #21267 and IG #20125; M.T.V. is supported by AIRC 5permille N. 21267 and patients are recruited through the GROM-L clinical network; E.B. was supported by the Francois Wallace Monahan Fellowship; E.P. is a Josie Robertson Investigator and is supported by the European Hematology Association, American Society of Hematology, Gabrielle's Angels Foundation, V Foundation and The Geoffrey Beene Foundation. We thank Tracey Iraca for logistic support.

bioRxiv preprint doi: https://doi.org/10.1101/2019.12.19.868844; this version posted December 19, 2019. The copyright holder for this preprint (which was not certified by peer review) is the author/funder, who has granted bioRxiv a license to display the preprint in perpetuity. It is made available under aCC-BY-NC-ND 4.0 International license.

REFERENCES

1. Kandoth, C. *et al.* Mutational landscape and significance across 12 major cancer types. *Nature* **502**, 333–339 (2013).
2. Zehir, A. *et al.* Mutational landscape of metastatic cancer revealed from prospective clinical sequencing of 10,000 patients. *Nat. Med.* **23**, 703–713 (2017).
3. Haase, D. *et al.* TP53 mutation status divides myelodysplastic syndromes with complex karyotypes into distinct prognostic subgroups. *Leukemia* **33**, 1747–1758 (2019).
4. Bejar, R. *et al.* Clinical effect of point mutations in myelodysplastic syndromes. *N. Engl. J. Med.* **364**, 2496–2506 (2011).
5. Haferlach, T. *et al.* Landscape of genetic lesions in 944 patients with myelodysplastic syndromes. *Leukemia* **28**, 241–247 (2014).
6. Kitagawa, M., Yoshida, S., Kuwata, T., Tanizawa, T. & Kamiyama, R. p53 expression in myeloid cells of myelodysplastic syndromes. Association with evolution of overt leukemia. *Am. J. Pathol.* **145**, 338–344 (1994).
7. Platzbecker, U. Treatment of MDS. *Blood* **133**, 1096–1107 (2019).
8. Lindsley, R. C. *et al.* Prognostic Mutations in Myelodysplastic Syndrome after Stem-Cell Transplantation. *N. Engl. J. Med.* **376**, 536–547 (2017).
9. Yoshizato, T. *et al.* Genetic abnormalities in myelodysplasia and secondary acute myeloid leukemia: impact on outcome of stem cell transplantation. *Blood* **129**, 2347–2358 (2017).
10. Jädersten, M. *et al.* TP53 mutations in low-risk myelodysplastic syndromes with del(5q) predict disease progression. *J. Clin. Oncol.* **29**, 1971–1979 (2011).
11. Rucker, F. G. *et al.* TP53 alterations in acute myeloid leukemia with complex karyotype

bioRxiv preprint doi: https://doi.org/10.1101/2019.12.19.868844; this version posted December 19, 2019. The copyright holder for this preprint (which was not certified by peer review) is the author/funder, who has granted bioRxiv a license to display the preprint in perpetuity. It is made available under aCC-BY-NC-ND 4.0 International license.

correlate with specific copy number alterations, monosomal karyotype, and dismal outcome. *Blood* **119**, 2114–2121 (2012).

12. Papaemmanuil, E. *et al.* Genomic Classification and Prognosis in Acute Myeloid Leukemia. *N. Engl. J. Med.* **374**, 2209–2221 (2016).
13. Wong, T. N. *et al.* Role of TP53 mutations in the origin and evolution of therapy-related acute myeloid leukaemia. *Nature* **518**, 552–555 (2015).
14. Greenberg, P. L. *et al.* Revised international prognostic scoring system for myelodysplastic syndromes. *Blood* **120**, 2454–2465 (2012).
15. Donehower, L. A. *et al.* Integrated Analysis of TP53 Gene and Pathway Alterations in The Cancer Genome Atlas. *Cell Rep.* **28**, 1370–1384.e5 (2019).
16. Kastenhuber, E. R. & Lowe, S. W. Putting p53 in Context. *Cell* **170**, 1062–1078 (2017).
17. de Vries, A. *et al.* Targeted point mutations of p53 lead to dominant-negative inhibition of wild-type p53 function. *Proc. Natl. Acad. Sci. U. S. A.* **99**, 2948–2953 (2002).
18. Boettcher, S. *et al.* A dominant-negative effect drives selection of TP53 missense mutations in myeloid malignancies. *Science* **365**, 599–604 (2019).
19. Schanz, J. *et al.* New comprehensive cytogenetic scoring system for primary myelodysplastic syndromes (MDS) and oligoblastic acute myeloid leukemia after MDS derived from an international database merge. *J. Clin. Oncol.* **30**, 820–829 (2012).
20. Breems, D. A. *et al.* Monosomal karyotype in acute myeloid leukemia: a better indicator of poor prognosis than a complex karyotype. *J. Clin. Oncol.* **26**, 4791–4797 (2008).
21. Grinfeld, J. *et al.* Classification and Personalized Prognosis in Myeloproliferative Neoplasms. *N. Engl. J. Med.* **379**, 1416–1430 (2018).
22. Papaemmanuil, E. *et al.* Clinical and biological implications of driver mutations in

bioRxiv preprint doi: https://doi.org/10.1101/2019.12.19.868844; this version posted December 19, 2019. The copyright holder for this preprint (which was not certified by peer review) is the author/funder, who has granted bioRxiv a license to display the preprint in perpetuity. It is made available under aCC-BY-NC-ND 4.0 International license.

myelodysplastic syndromes. *Blood* **122**, 3616–27; quiz 3699 (2013).

23. Chakravarty, D. *et al.* OncoKB: A Precision Oncology Knowledge Base. *JCO Precis Oncol* **2017**, (2017).
24. Tate, J. G. *et al.* COSMIC: the Catalogue Of Somatic Mutations In Cancer. *Nucleic Acids Res.* **47**, D941–D947 (2019).
25. Bouaoun, L. *et al.* TP53 Variations in Human Cancers: New Lessons from the IARC TP53 Database and Genomics Data. *Hum. Mutat.* **37**, 865–876 (2016).
26. Ptashkin, R. N. *et al.* Abstract 3409: MSK-IMPACT Heme: Validation and clinical experience of a comprehensive molecular profiling platform for hematologic malignancies. *Molecular and Cellular Biology / Genetics* (2019). doi:10.1158/1538-7445.sabcs18-3409
27. Karczewski, K. J. *et al.* Variation across 141,456 human exomes and genomes reveals the spectrum of loss-of-function intolerance across human protein-coding genes: Supplementary Information. doi:10.1101/531210
28. Landrum, M. J. *et al.* ClinVar: public archive of relationships among sequence variation and human phenotype. *Nucleic Acids Res.* **42**, D980–5 (2014).
29. Nik-Zainal, S. *et al.* The life history of 21 breast cancers. *Cell* **149**, 994–1007 (2012).
30. Sallman, D. A. *et al.* Impact of TP53 mutation variant allele frequency on phenotype and outcomes in myelodysplastic syndromes. *Leukemia* **30**, 666–673 (2016).
31. Lausen, B. & Schumacher, M. Maximally Selected Rank Statistics. *Biometrics* **48**, 73 (1992).
32. Levine, A. J. The many faces of p53: something for everyone. *J. Mol. Cell Biol.* (2019). doi:10.1093/jmcb/mjz026
33. Lang, G. A. *et al.* Gain of Function of a p53 Hot Spot Mutation in a Mouse Model of Li-Fraumeni Syndrome. *Cell* **119**, 861–872 (2004).

bioRxiv preprint doi: https://doi.org/10.1101/2019.12.19.868844; this version posted December 19, 2019. The copyright holder for this preprint (which was not certified by peer review) is the author/funder, who has granted bioRxiv a license to display the preprint in perpetuity. It is made available under aCC-BY-NC-ND 4.0 International license.

34. Olive, K. P. *et al.* Mutant p53 Gain of Function in Two Mouse Models of Li-Fraumeni Syndrome. *Cell* **119**, 847–860 (2004).

35. Loizou, E. *et al.* A Gain-of-Function p53-Mutant Oncogene Promotes Cell Fate Plasticity and Myeloid Leukemia through the Pluripotency Factor FOXH1. *Cancer Discov.* **9**, 962–979 (2019).

36. Roman, E. *et al.* Myeloid malignancies in the real-world: Occurrence, progression and survival in the UK's population-based Haematological Malignancy Research Network 2004–15. *Cancer Epidemiology* **42**, 186–198 (2016).

37. Smith, A. *et al.* Cohort Profile: The Haematological Malignancy Research Network (HMRN); a UK population-based patient cohort. *Int. J. Epidemiol.* (2018). doi:10.1093/ije/dyy044

38. Welch, J. S. *et al.* TP53 and Decitabine in Acute Myeloid Leukemia and Myelodysplastic Syndromes. *N. Engl. J. Med.* **375**, 2023–2036 (2016).

39. Collins, F. S. & Varmus, H. A New Initiative on Precision Medicine. *New England Journal of Medicine* **372**, 793–795 (2015).

40. Olivier, M., Hollstein, M. & Hainaut, P. TP53 Mutations in Human Cancers: Origins, Consequences, and Clinical Use. *Cold Spring Harbor Perspectives in Biology* **2**, a001008–a001008 (2010).

41. International Standing Committee on Human Cytogenetic Nomenclature. *ISCN 2013: An International System for Human Cytogenetic Nomenclature (2013)*. (Karger Medical and Scientific Publishers, 2013).

42. Li, H. & Durbin, R. Fast and accurate long-read alignment with Burrows-Wheeler transform. *Bioinformatics* **26**, 589–595 (2010).

43. Cibulskis, K. *et al.* Sensitive detection of somatic point mutations in impure and

bioRxiv preprint doi: https://doi.org/10.1101/2019.12.19.868844; this version posted December 19, 2019. The copyright holder for this preprint (which was not certified by peer review) is the author/funder, who has granted bioRxiv a license to display the preprint in perpetuity. It is made available under aCC-BY-NC-ND 4.0 International license.

heterogeneous cancer samples. *Nat. Biotechnol.* **31**, 213–219 (2013).

44. Saunders, C. T. *et al.* Strelka: accurate somatic small-variant calling from sequenced tumor-normal sample pairs. *Bioinformatics* **28**, 1811–1817 (2012).
45. Ye, K., Schulz, M. H., Long, Q., Apweiler, R. & Ning, Z. Pindel: a pattern growth approach to detect break points of large deletions and medium sized insertions from paired-end short reads. *Bioinformatics* **25**, 2865–2871 (2009).
46. Karczewski, K. J. *et al.* Variation across 141,456 human exomes and genomes reveals the spectrum of loss-of-function intolerance across human protein-coding genes. doi:10.1101/531210
47. Thorvaldsdóttir, H., Robinson, J. T. & Mesirov, J. P. Integrative Genomics Viewer (IGV): high-performance genomics data visualization and exploration. *Brief. Bioinform.* **14**, 178–192 (2013).
48. Cerami, E. *et al.* The cBio cancer genomics portal: an open platform for exploring multidimensional cancer genomics data. *Cancer Discov.* **2**, 401–404 (2012).
49. Chang, M. T. *et al.* Identifying recurrent mutations in cancer reveals widespread lineage diversity and mutational specificity. *Nat. Biotechnol.* **34**, 155–163 (2016).
50. Chang, M. T. *et al.* Accelerating Discovery of Functional Mutant Alleles in Cancer. *Cancer Discov.* **8**, 174–183 (2018).
51. Giacomelli, A. O. *et al.* Mutational processes shape the landscape of TP53 mutations in human cancer. *Nat. Genet.* **50**, 1381–1387 (2018).
52. Talevich, E., Shain, A. H., Botton, T. & Bastian, B. C. CNVkit: Genome-Wide Copy Number Detection and Visualization from Targeted DNA Sequencing. *PLoS Comput. Biol.* **12**, e1004873 (2016).

bioRxiv preprint doi: https://doi.org/10.1101/2019.12.19.868844; this version posted December 19, 2019. The copyright holder for this preprint (which was not certified by peer review) is the author/funder, who has granted bioRxiv a license to display the preprint in perpetuity. It is made available under aCC-BY-NC-ND 4.0 International license.

FIGURES AND EXTENDED DATA LEGENDS

Figure 1 | Integration of *TP53* mutations and allelic imbalances at the *TP53* locus identifies *TP53* states with evidence of mono-allelic or bi-allelic targeting.

Figure 2 | Genome instability within the multi-hit *TP53* subgroups but not the mono-allelic subgroup.

Figure 3 | *TP53* allelic state associates with distinct clinical phenotypes.

Figure 4 | *TP53* allelic state shapes patient outcomes.

Figure 5 | *TP53* allelic state demarcates distinct outcomes in therapy-related MDS and on different therapies.

Figure 6 | Clinical workflow for the assessment of *TP53* allelic state.

Extended Data Figure 1 | Landscape of chromosomal aberrations in MDS.

Extended Data Figure 2 | Evidence of bi-allelic *TP53* targeting in the cases with multiple *TP53* mutations.

Extended Data Figure 3 | Heatmap of chromosomal aberrations per *TP53* allelic state.

Extended Data Figure 4 | Representation of WHO subtypes and IPSS-R risk groups per *TP53* allelic state.

Extended Data Figure 5 | Outcomes across *TP53* subgroups.

Extended Data Figure 6 | *TP53* allelic state segregates patient outcomes across WHO subtypes and IPSS-R risk groups.

Extended Data Figure 7 | Maintained differences in genome instability levels and outcomes per *TP53* state across mutation types.

Extended Data Table 1 | Study cohort characteristics.

Extended Data Table 2 | Validation cohort characteristics.

Extended Data Table 3 | Characteristics of treated cohort subsets.

bioRxiv preprint doi: https://doi.org/10.1101/2019.12.19.868844; this version posted December 19, 2019. The copyright holder for this preprint (which was not certified by peer review) is the author/funder, who has granted bioRxiv a license to display the preprint in perpetuity. It is made available under aCC-BY-NC-ND 4.0 International license.

Figure 1 | Integration of *TP53* mutations and allelic imbalances at the *TP53* locus identifies *TP53* states with evidence of mono-allelic or bi-allelic targeting. a, Number of patients (from patients with any hit at the *TP53* locus) with 0, 1, 2 or 3 *TP53* mutations. Colors represent the status of chromosome 17 at the *TP53* locus, to include copy-neutral loss of heterozygosity (cnloh), deletion (del), isochromosome 17q rearrangement (iso17q), gain or no detected aberration (normal). **b,** Frequency of *TP53* subgroups within *TP53*-mutated patients. *TP53* subgroups are defined as cases with i) single gene mutation (1mut) ii) several mutations with normal status of chromosome 17 at the *TP53* locus (>1mut) iii) mutation(s) and chromosomal deletion at the *TP53* locus (mut+del) and iv) mutation(s) and copy-neutral loss of heterozygosity at the *TP53* locus (mut+cnloh). **c,** Density estimation of variant allele frequency (VAF) of *TP53* mutations across *TP53* subgroups (1mut, >1mut, mut+del, mut+cnloh from top to bottom). **d,** Distribution of *TP53* mutations along the gene body. Mutations from patients with mono-allelic *TP53* per single gene mutation are depicted at the top, mutations from patients with multiple *TP53* hits at the bottom. Missense mutations are shown as green circles. Truncated mutations, including nonsense or nonstop mutations, frameshift deletions or insertions and splice site variants are shown as pink circles. Other types of mutations to include inframe deletions or insertions are shown as orange circles. TAD: transactivation domain; DBD: DNA binding domain; OD: oligomerization domain.

bioRxiv preprint doi: https://doi.org/10.1101/2019.12.19.868844; this version posted December 19, 2019. The copyright holder for this preprint (which was not certified by peer review) is the author/funder, who has granted bioRxiv a license to display the preprint in perpetuity. It is made available under aCC-BY-NC-ND 4.0 International license.

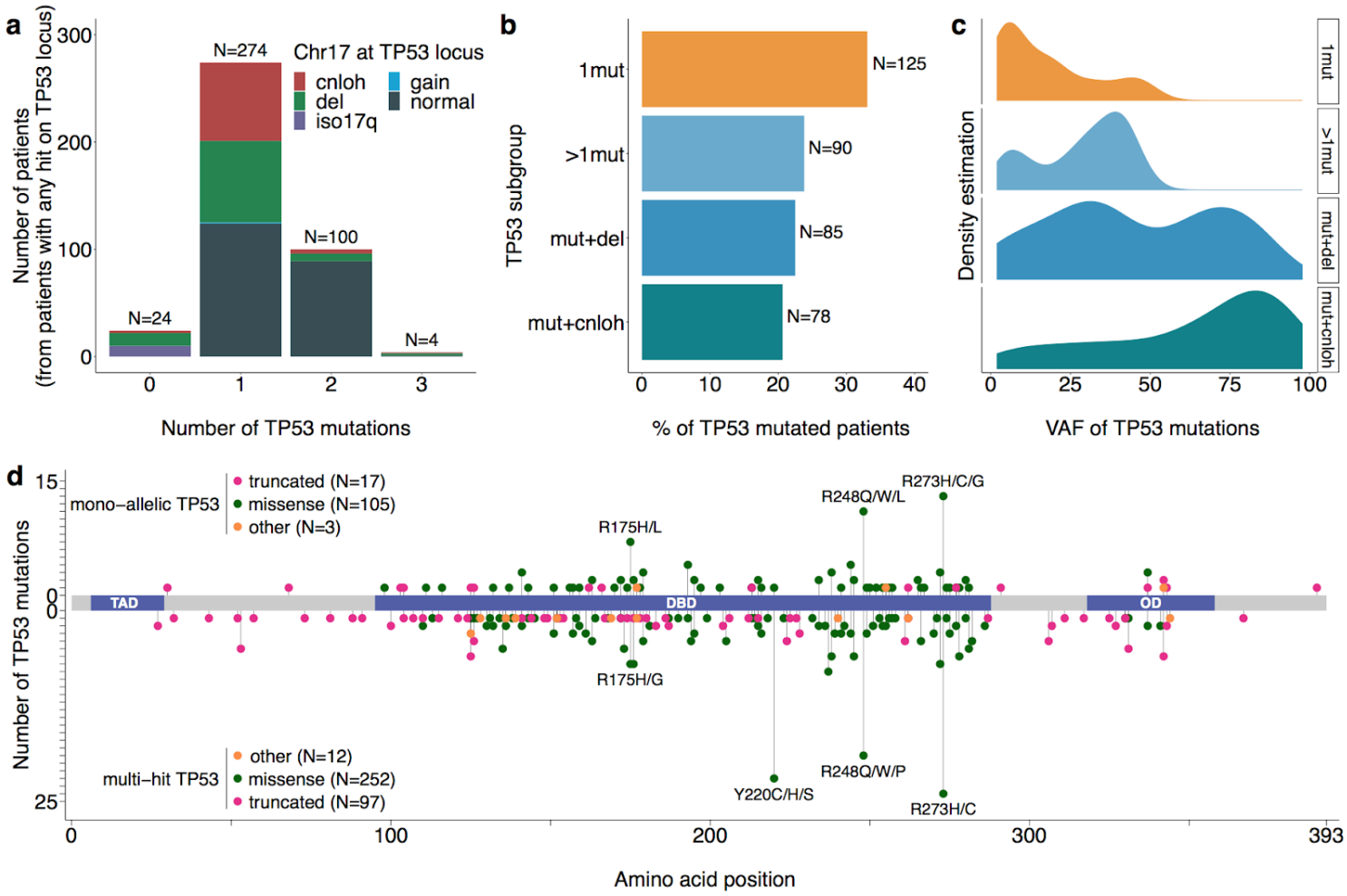

bioRxiv preprint doi: https://doi.org/10.1101/2019.12.19.868844; this version posted December 19, 2019. The copyright holder for this preprint (which was not certified by peer review) is the author/funder, who has granted bioRxiv a license to display the preprint in perpetuity. It is made available under aCC-BY-NC-ND 4.0 International license.

Figure 2 | Genome instability within the multi-hit *TP53* subgroups but not the mono-allelic subgroup. a, Distribution of the number of chromosomal aberrations on other chromosomes than 17 per patient across *TP53* subgroups and types of aberrations, i.e., rearrangement (rearr), gain or deletion (del). ****p<0.0001, Wilcoxon rank-sum test, each compared to the same aberration within the 1mut group. **b,** Number of unique chromosomes other than 17 affected by a chromosomal aberration (rearrangement, deletion or gain) per *TP53* subgroup. Dots represent the median across patients and lines extend from 25% to 75% quantiles. ****p<0.0001, Wilcoxon rank-sum test, compared to the 1mut group. **c,** Interaction between *TP53* allelic state and complex karyotype. 13% (16/125) of mono-allelic *TP53* patients (1mut) had a complex karyotype. Conversely, 91% (231/253) of multi-hit *TP53* patients (multi) had a complex karyotype (OR=70, 95% CI: 33-150, $p<10^{-16}$ Fisher exact test).

bioRxiv preprint doi: https://doi.org/10.1101/2019.12.19.868844; this version posted December 19, 2019. The copyright holder for this preprint (which was not certified by peer review) is the author/funder, who has granted bioRxiv a license to display the preprint in perpetuity. It is made available under aCC-BY-NC-ND 4.0 International license.

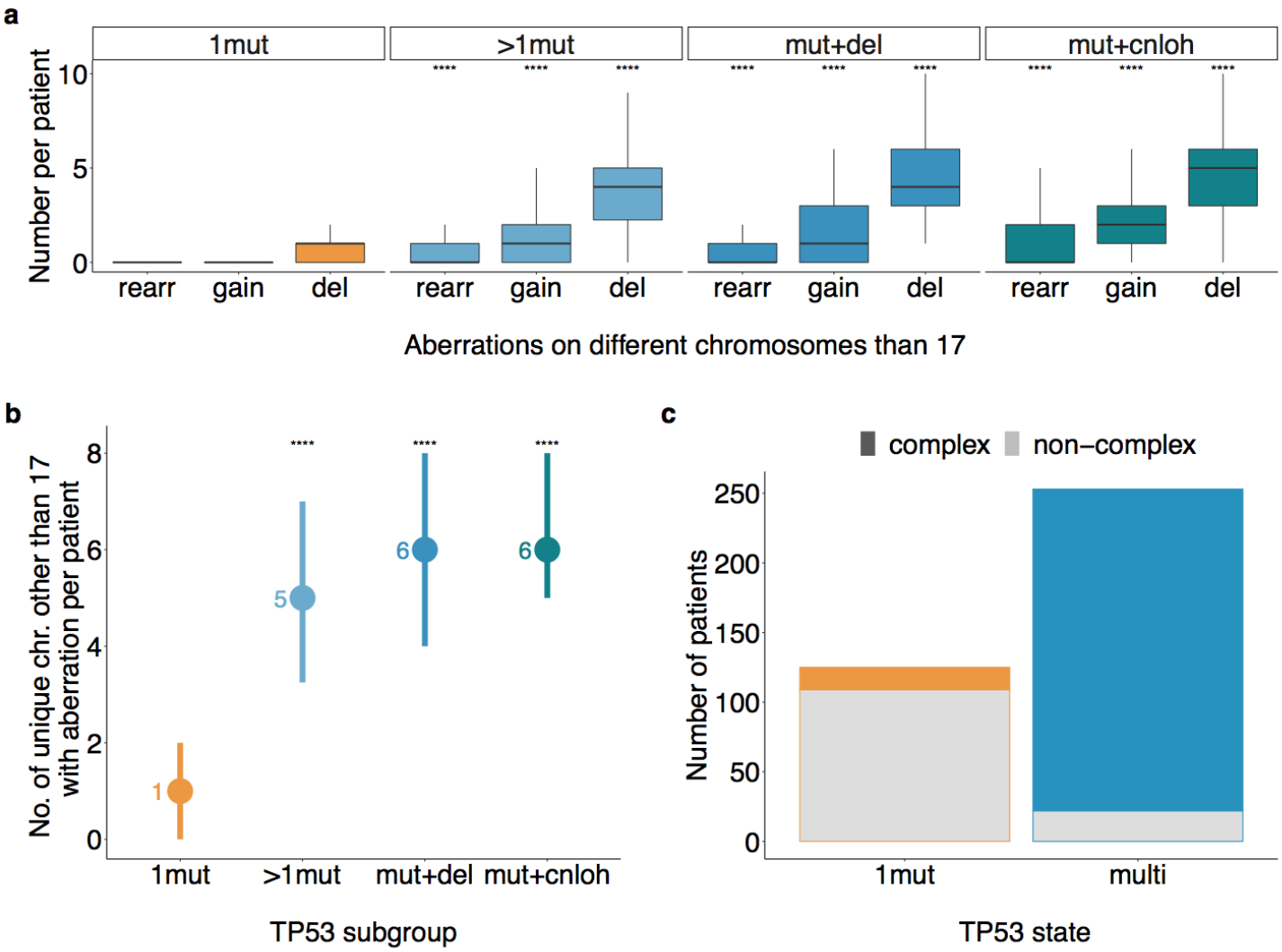

bioRxiv preprint doi: https://doi.org/10.1101/2019.12.19.868844; this version posted December 19, 2019. The copyright holder for this preprint (which was not certified by peer review) is the author/funder, who has granted bioRxiv a license to display the preprint in perpetuity. It is made available under aCC-BY-NC-ND 4.0 International license.

Figure 3 | *TP53* allelic state associates with distinct clinical phenotypes. a-c. Boxplots indicative of the levels of cytopenias per *TP53* state of single gene mutation (1mut) or multiple hits (multi), respectively hemoglobin in panel a., platelets in panel b. and absolute neutrophil count (ANC) in panel c. Black lines represent the median across patients and filled boxes extend from 25% to 75% quantiles. The y-axis are square-root transformed. **d.** Percentage of bone marrow blasts per *TP53* state of a single gene mutation (1mut) or multiple hits (multi). ***p<0.001, ****p<0.0001, Wilcoxon rank-sum test.

bioRxiv preprint doi: https://doi.org/10.1101/2019.12.19.868844; this version posted December 19, 2019. The copyright holder for this preprint (which was not certified by peer review) is the author/funder, who has granted bioRxiv a license to display the preprint in perpetuity. It is made available under aCC-BY-NC-ND 4.0 International license.

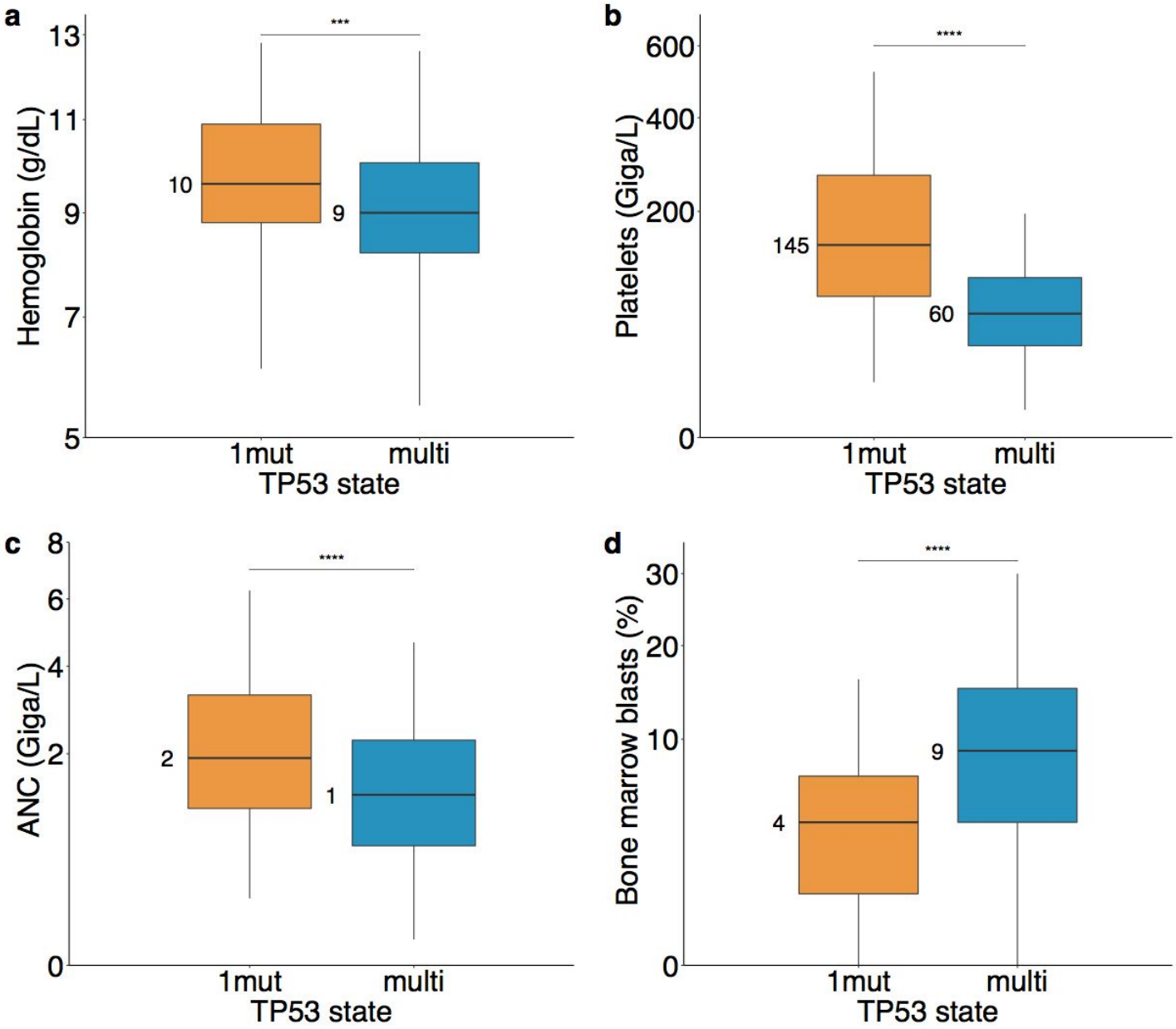

bioRxiv preprint doi: https://doi.org/10.1101/2019.12.19.868844; this version posted December 19, 2019. The copyright holder for this preprint (which was not certified by peer review) is the author/funder, who has granted bioRxiv a license to display the preprint in perpetuity. It is made available under aCC-BY-NC-ND 4.0 International license.

Figure 4 | *TP53* allelic state shapes patient outcomes. Kaplan-Meier probability estimates of overall survival **(a)** and cumulative incidence of AML transformation (AMLt) **(b)** per *TP53* state of wild-type *TP53* (WT), mono-allelic *TP53* per single gene mutation (1mut) and multiple *TP53* hits (multi). **c,** Results of Cox proportional hazards regression for overall survival (OS) performed on 2,719 patients with complete data for OS and with 1,290 observed death. Explicative variables are Hemoglobin, Platelets, Absolute neutrophil count (ANC), Bone marrow blasts, Cytogenetic IPSS-R risk scores (very-good, good, intermediate is the reference, poor and very-poor) and *TP53* allelic state (mono-allelic, multi-hit and wild-type is the reference). Hemoglobin, Platelets, ANC and Bone marrow blasts are scaled by their sample mean. Age is scaled by a factor 10. The x-axis is $\log_{10}$ scaled. **d,** Results of cause-specific Cox proportional hazards regression for AML transformation (AMLt) performed on 2,464 patients with complete data for AMLt and with 411 observed transformation. Covariates are the same as in c. The x-axis is $\log_{10}$ scaled. ****p<0.0001, ***p<0.001, **p<0.01, *p<0.05 Wald test.

bioRxiv preprint doi: https://doi.org/10.1101/2019.12.19.868844; this version posted December 19, 2019. The copyright holder for this preprint (which was not certified by peer review) is the author/funder, who has granted bioRxiv a license to display the preprint in perpetuity. It is made available under aCC-BY-NC-ND 4.0 International license.

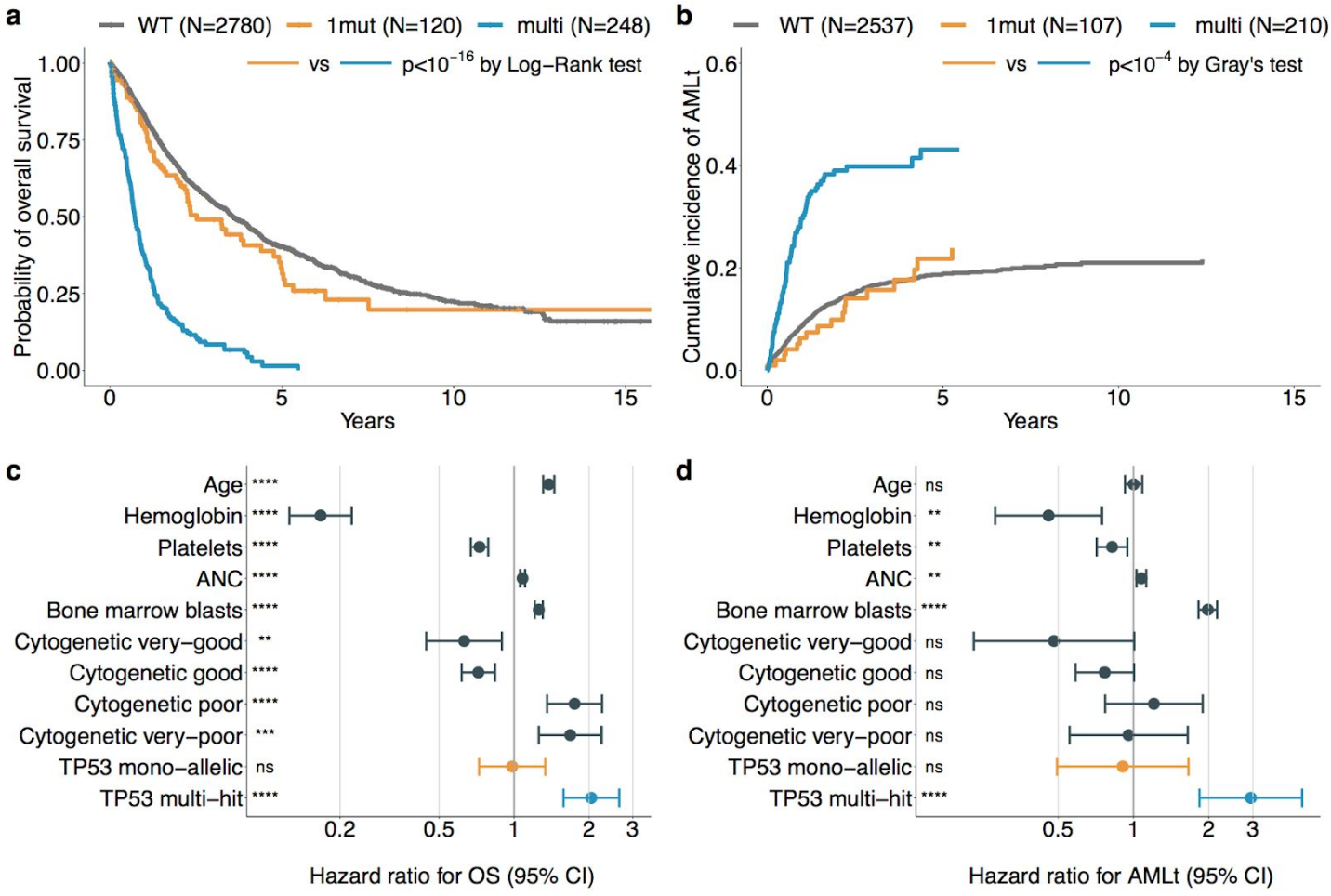

bioRxiv preprint doi: https://doi.org/10.1101/2019.12.19.868844; this version posted December 19, 2019. The copyright holder for this preprint (which was not certified by peer review) is the author/funder, who has granted bioRxiv a license to display the preprint in perpetuity. It is made available under aCC-BY-NC-ND 4.0 International license.

Figure 5 | *TP53* allelic state demarcates distinct outcomes in therapy-related MDS and on different therapies. a, Kaplan-Meier probability estimates of overall survival per allelic state of wild-type *TP53* (WT), mono-allelic *TP53* per single gene mutation (1mut) and multiple *TP53* hits (multi); and across type of MDS, i.e., de-novo MDS (solid line) or therapy-related MDS (dashed line). Within the therapy-related cases, 10 had a mono-allelic *TP53* mutation (dashed orange line), 52 were multi-hit *TP53* (dashed blue line) and 162 were *TP53* wild-type (dashed grey line). **b-c-d**, Kaplan-Meier probability estimates of overall survival post start of hypomethylating agent (HMA) treatment **(b)** start of Lenalidomide treatment for patients with del(5q) **(c)** hematopoietic stem cell transplantation (HSCT) **(d)** per allelic state of wild-type *TP53* (WT), mono-allelic *TP53* (1mut) and multiple *TP53* hits (multi). In b, c, and d, overall survival was measured from the time of treatment start or HSCT to the time of death from any cause. Patients alive at the last follow-up date were censored at that time. Annotated p-values are from the log-rank test.

bioRxiv preprint doi: https://doi.org/10.1101/2019.12.19.868844; this version posted December 19, 2019. The copyright holder for this preprint (which was not certified by peer review) is the author/funder, who has granted bioRxiv a license to display the preprint in perpetuity. It is made available under aCC-BY-NC-ND 4.0 International license.

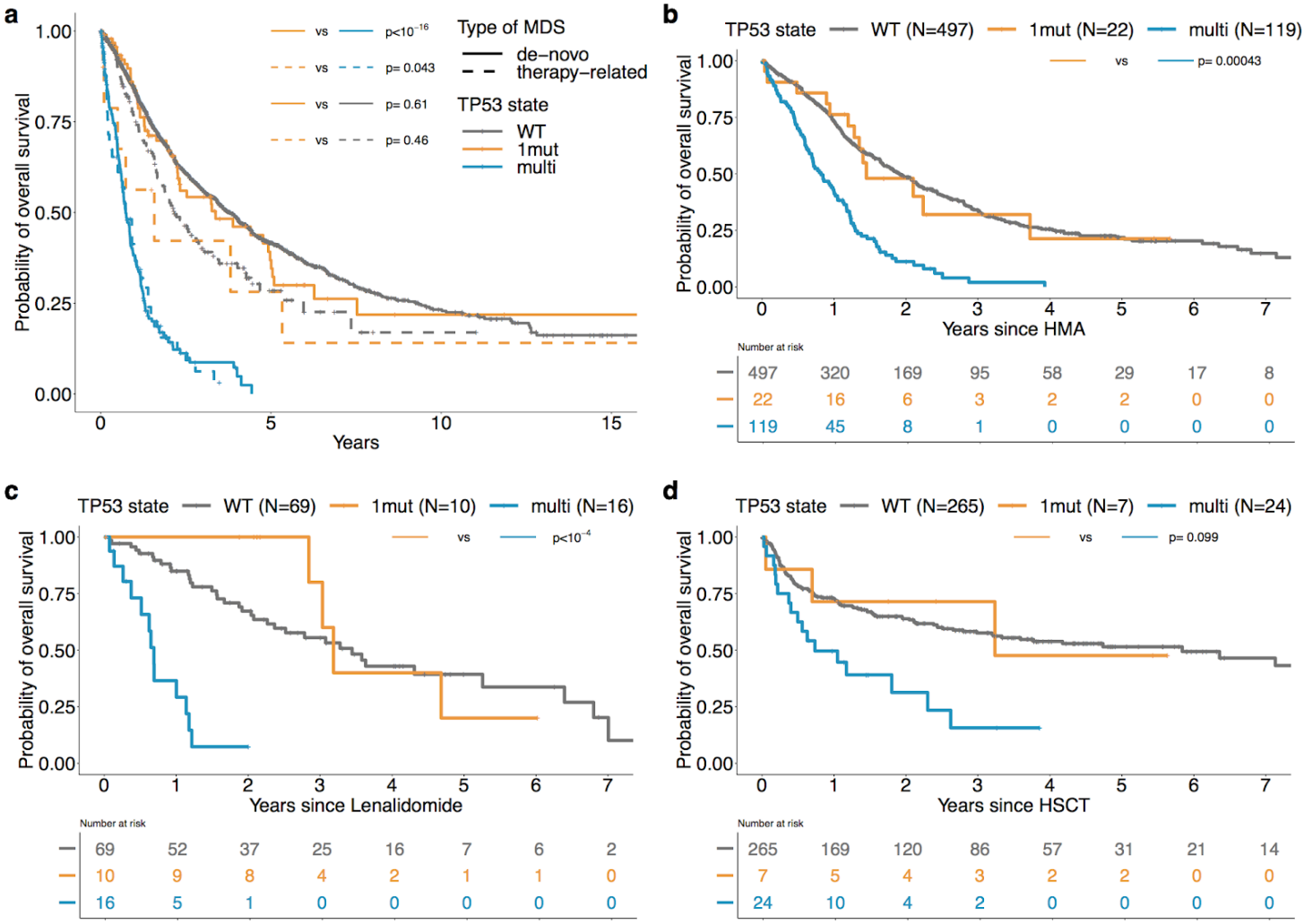

bioRxiv preprint doi: https://doi.org/10.1101/2019.12.19.868844; this version posted December 19, 2019. The copyright holder for this preprint (which was not certified by peer review) is the author/funder, who has granted bioRxiv a license to display the preprint in perpetuity. It is made available under aCC-BY-NC-ND 4.0 International license.

Figure 6 | Clinical workflow for the assessment of *TP53* allelic state. Schematic of a simple clinical workflow based on the number of *TP53* mutations, the presence or absence of deletion 17p per cytogenetic analysis, and the presence or absence of cnLOH at 17p or focal deletion per NGS based assay or SNP array. Mutations were considered if VAF≥2%. VAF: variant allele frequency; CK: complex karyotype; OS: overall survival; AML: transformation to acute myeloid leukemia.

bioRxiv preprint doi: https://doi.org/10.1101/2019.12.19.868844; this version posted December 19, 2019. The copyright holder for this preprint (which was not certified by peer review) is the author/funder, who has granted bioRxiv a license to display the preprint in perpetuity. It is made available under aCC-BY-NC-ND 4.0 International license.

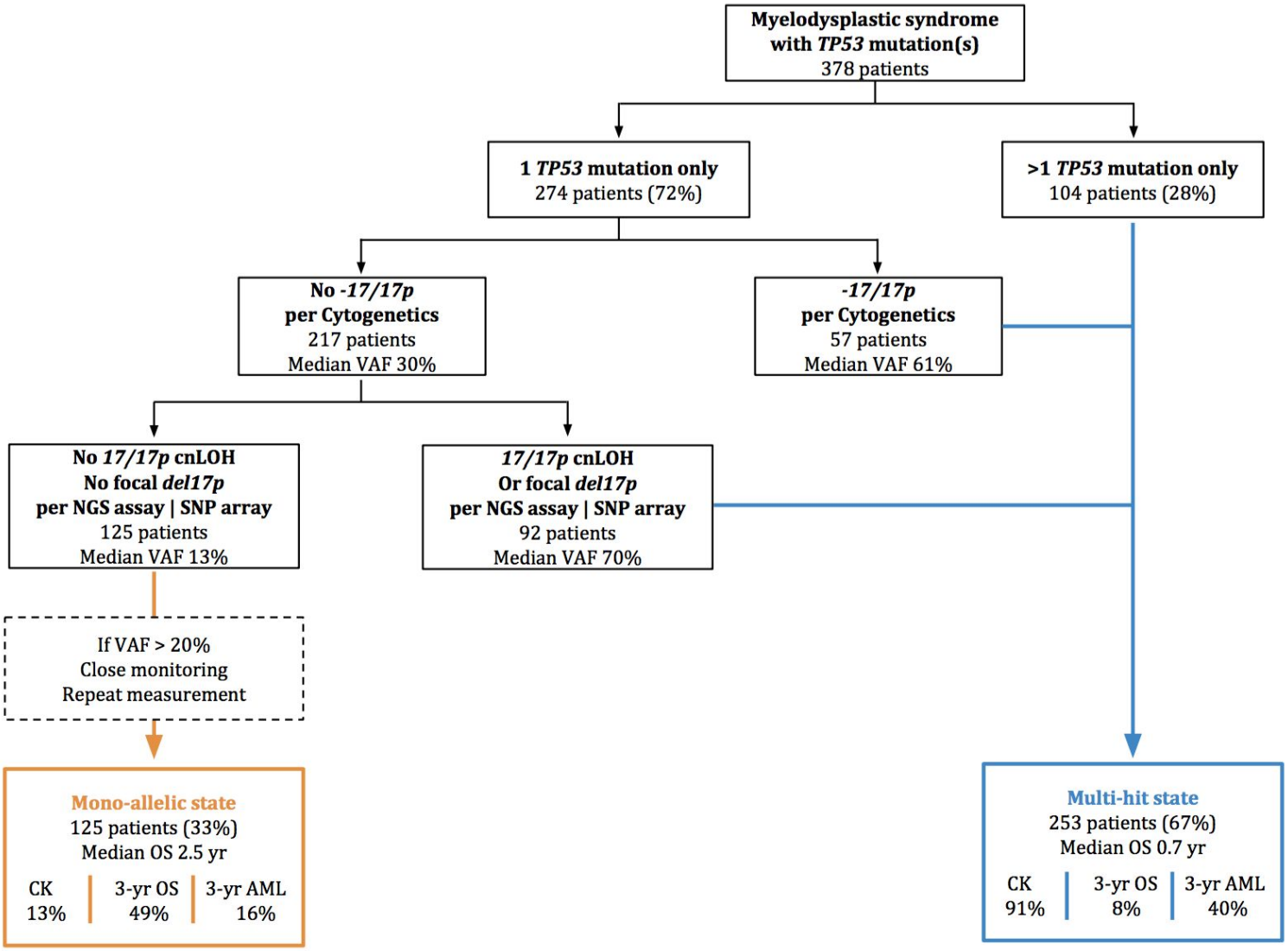

bioRxiv preprint doi: https://doi.org/10.1101/2019.12.19.868844; this version posted December 19, 2019. The copyright holder for this preprint (which was not certified by peer review) is the author/funder, who has granted bioRxiv a license to display the preprint in perpetuity. It is made available under aCC-BY-NC-ND 4.0 International license.

Extended Data Figure 1 | Landscape of chromosomal aberrations in MDS. a. Landscape of chromosomal arm-level aberrations across 3,324 patients. Aberrations include copy-neutral loss-of-heterozygosity (cnloh), deletion (del) and gain. The x-axis indicates chromosome arms or entire chromosomes affected by aberrations. Aberrations were assessed using the integration of conventional G-banding analysis (CBA) data and NGS derived copy-number profiles. NGS aberrant segments were restricted to segments larger than 3 megabases. **b.** Frequency distribution of chromosomal aberrations across 3,324 patients ordered by type of aberrations. First top three plots represent arm-level copy-neutral loss-of-heterozygosity (cnloh), deletion (del) and gain. Fourth bottom plot represents other types of aberrations to include the presence of marker chromosome (mar), rearrangements where r_i_j denotes a rearrangement between chromosome i and j, isochromosome 17q (iso17q), whole genome amplification (WGA) and presence of ring chromosome (ring). All aberrations observed in more than 2 patients are depicted. Of note, cnloh is detectable with NGS but not with CBA. On the opposite, rearrangements, presence of marker or ring chromosome and WGA were only assessed from CBA data. On the 393 cases with missing CBA data, those specific aberrations were imputed from other molecular markers.

bioRxiv preprint doi: https://doi.org/10.1101/2019.12.19.868844; this version posted December 19, 2019. The copyright holder for this preprint (which was not certified by peer review) is the author/funder, who has granted bioRxiv a license to display the preprint in perpetuity. It is made available under aCC-BY-NC-ND 4.0 International license.

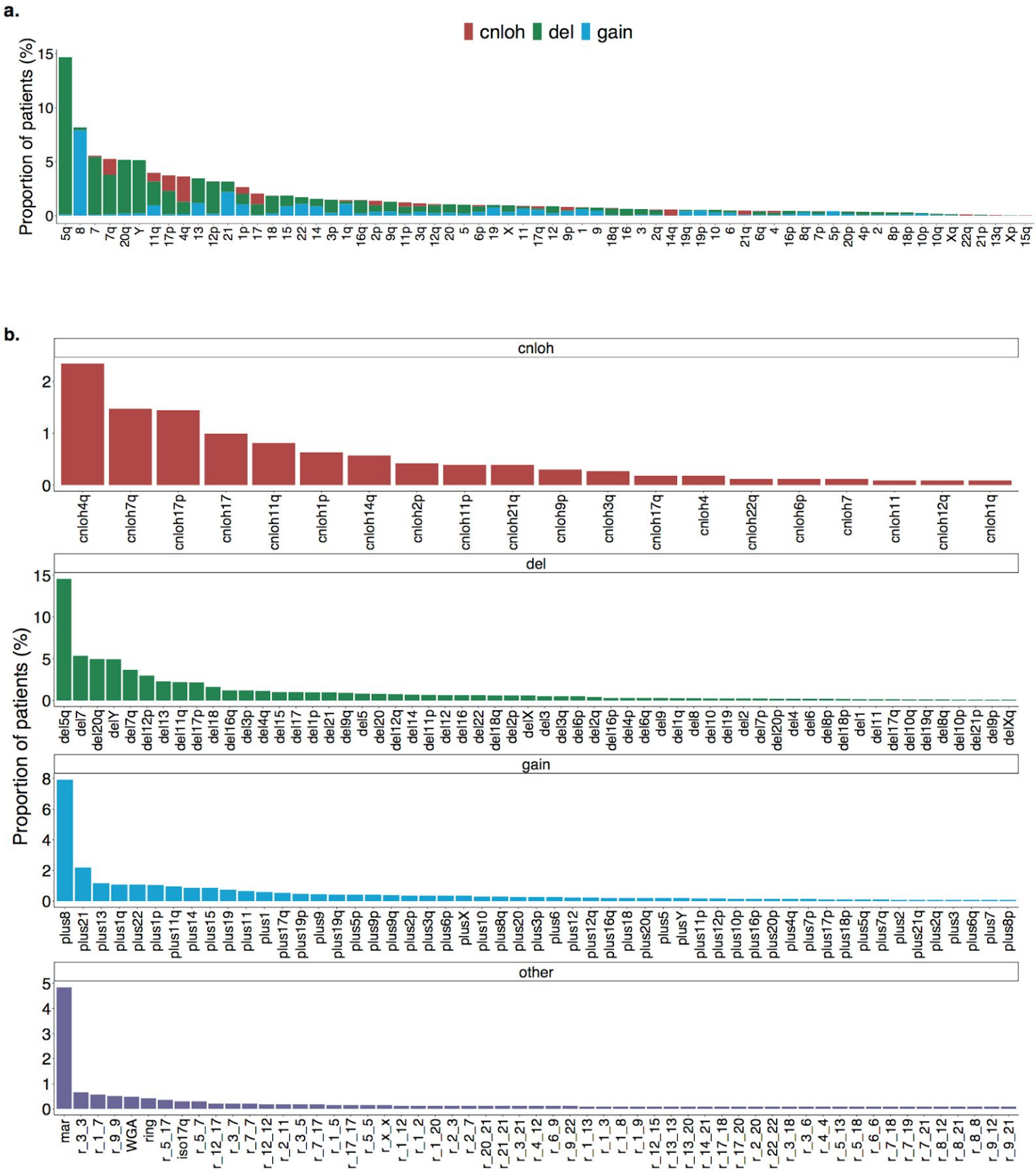

bioRxiv preprint doi: https://doi.org/10.1101/2019.12.19.868844; this version posted December 19, 2019. The copyright holder for this preprint (which was not certified by peer review) is the author/funder, who has granted bioRxiv a license to display the preprint in perpetuity. It is made available under aCC-BY-NC-ND 4.0 International license.

Extended Data Figure 2 | Evidence of bi-allelic *TP53* targeting in the cases with multiple *TP53* mutations. a. Scatter plot of the two maximum *TP53* variant allele frequency (VAF) values from the cases with multiple *TP53* mutations and no copy-neutral loss-of-heterozygosity or deletion (N=90). Points are annotated according to the level of information of the mutation pairs. If the sum of the two VAFs exceeded 50%, the mutations were considered to be in the same cells, which happened in 67% (n=60) of the cases (triangle and diamond points). In some specific cases where the genomic distance between two mutations was smaller than the read length, it was possible to phase the mutations. In the 18 cases where possible to assess, mutations were all observed to be unphased, i.e., in trans (square and diamond points). Within those 18 pairs of unphased mutations, 10 pairs had a sum of VAFs above 50%, i.e., mutations were necessarily on different alleles and in the same cells, implying bi-allelic targeting (diamond points). **b.** Table of pairs of *TP53* mutations from the same patients that could be phased. All pairs were in trans, i.e., mutations were supported by different alleles. **c.** Representative IGV example of unphased mutations (patient p12 from table b.).

bioRxiv preprint doi: https://doi.org/10.1101/2019.12.19.868844; this version posted December 19, 2019. The copyright holder for this preprint (which was not certified by peer review) is the author/funder, who has granted bioRxiv a license to display the preprint in perpetuity. It is made available under aCC-BY-NC-ND 4.0 International license.

a.

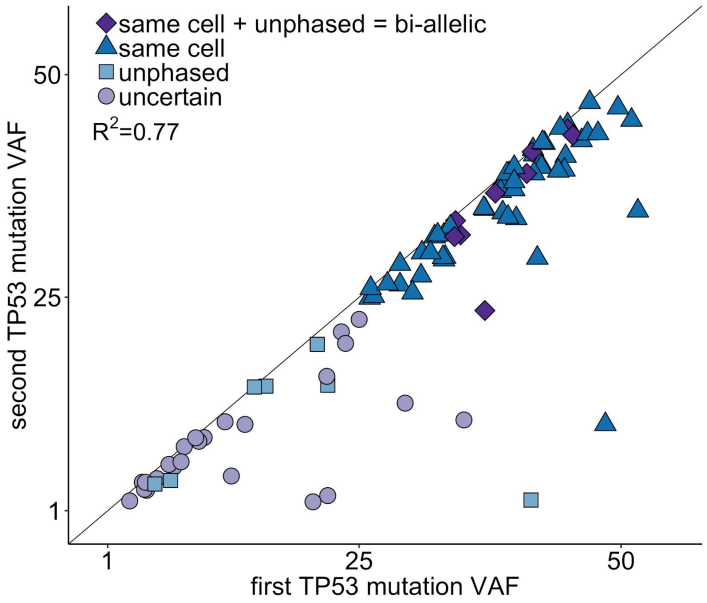

b.

Patient	TP53 Variant 1	Protein Change 1	VAF 1	TP53 Variant 2	Protein Change 2	VAF 2	note
p1	17_7577498_C_T	p.?	0.37	17_7577529_A_T	p.I251N	0.24	
p2	17_7578176_C_T	p.?	0.22	17_7578190_T_C	p.Y220C	0.15	
p3	17_7577538_C_T	p.R248Q	0.16	17_7577570_C_T	p.M237I	0.04	third splice-site mutation at VAF 0.16
p4	17_7577498_C_T	p.?	0.21	17_7577515_T_G	p.T256P	0.2	
p5	17_7577520_A_T	p.I254N	0.46	17_7577539_G_A	p.R248W	0.43	
p6	17_7577106_G_C	p.P278A	0.41	17_7577120_C_T	p.R273H	0.02	
p7	17_7578190_T_C	p.Y220C	0.34	17_7578268_A_C	p.L194R	0.34	
p8	17_7577536_T_A	p.R249W	0.39	17_7577568_C_T	p.C238Y	0.41	
p9	17_7578442_T_C	p.Y163C	0.39	17_7578538_T_A	p.N131I	0.38	
p10	17_7579312_C_T	p.T125T	0.15	17_7579349_A_C	p.F113C	0.15	
p11	17_7578392_C_A	p.E180*	0.05	17_7578403_C_T	p.C176Y	0.06	
p12	17_7578190_T_C	p.Y220C	0.45	17_7578191_A_G	p.Y220H	0.44	
p13	17_7577538_C_T	p.R248Q	0.34	17_7577570_C_T	p.M237I	0.32	
p14	17_7578460_A_C	p.V157G	0.15	17_7578478_G_C	p.P151R	0.65	
p15	17_7578455_C_G	p.A159P	0.04	17_7578524_G_C	p.Q136E	0.07	
p16	17_7577018_C_T	p.?	0.38	17_7577097_C_A	p.D281Y	0.37	
p17	17_7578394_T_A	p.H179L	0.42	17_7578415_AC_A	p.V172fs*2	0.41	
p18	17_7579311_C_T	p.?	0.32	17_7579358_CG_C	p.R110fs*13	0.35	

c.

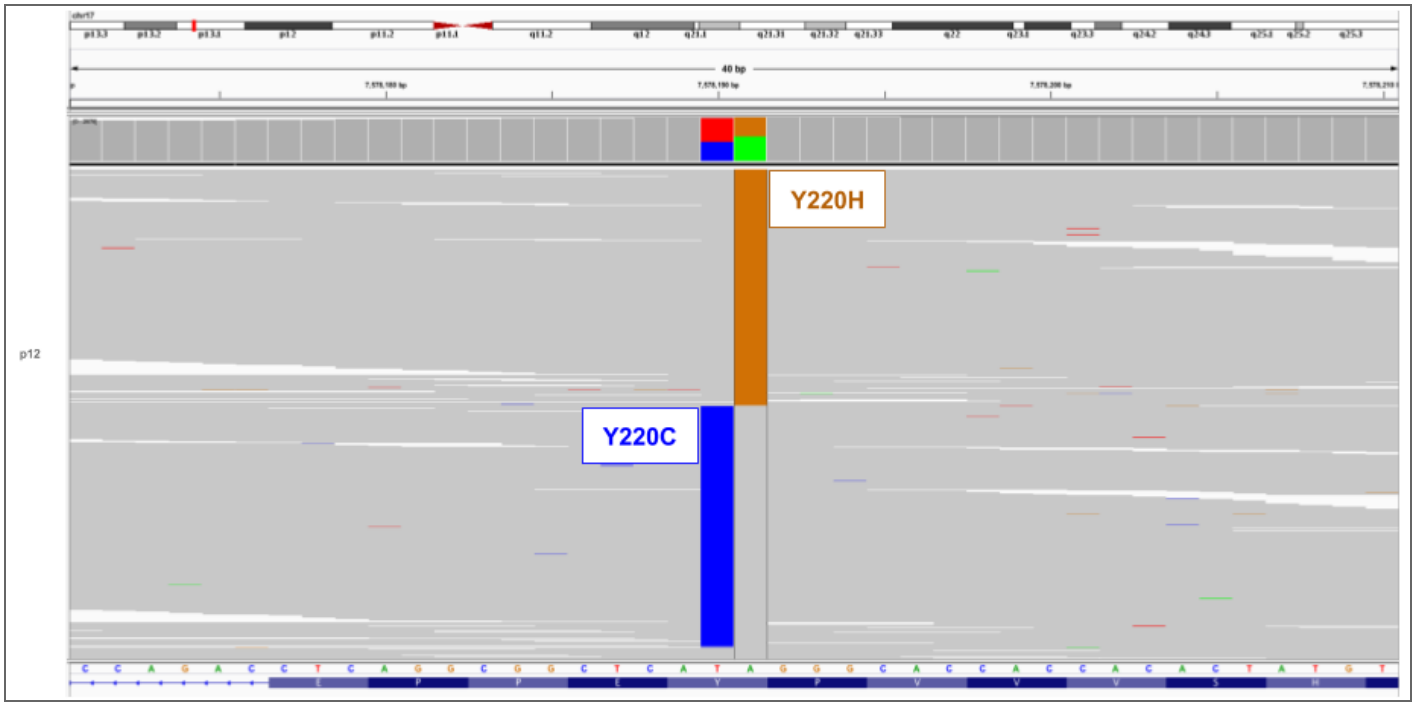

bioRxiv preprint doi: https://doi.org/10.1101/2019.12.19.868844; this version posted December 19, 2019. The copyright holder for this preprint (which was not certified by peer review) is the author/funder, who has granted bioRxiv a license to display the preprint in perpetuity. It is made available under aCC-BY-NC-ND 4.0 International license.

Extended Data Figure 3 | Heatmap of chromosomal aberrations per *TP53* allelic state. Each column represents a patient from the *TP53* subgroups of single gene mutation (top orange band, 1mut), multiple mutations (top light blue band, >1mut), mutation(s) and deletion (top blue band, mut+del) and mutation(s) and copy-neutral loss of heterozygosity (top dark blue band, mut+cnloh). Aberrations observed at a frequency higher than 2% in either mono-allelic or multi-hit *TP53* state are depicted on the y-axis. Aberrations include from top to bottom the annotation of complex karyotype (complex), the presence of marker chromosome (mar), deletion (del), gain (plus), rearrangement (with r_i_j rearrangement between chromosome i and j), copy-neutral loss of heterozygosity (cnloh), whole genome amplification (WGA) and the presence of ring chromosome (ring). Note that the deletions of 17p of two cases from the 1mut *TP53* subgroup did not affect the *TP53* locus.

bioRxiv preprint doi: https://doi.org/10.1101/2019.12.19.868844; this version posted December 19, 2019. The copyright holder for this preprint (which was not certified by peer review) is the author/funder, who has granted bioRxiv a license to display the preprint in perpetuity. It is made available under aCC-BY-NC-ND 4.0 International license.

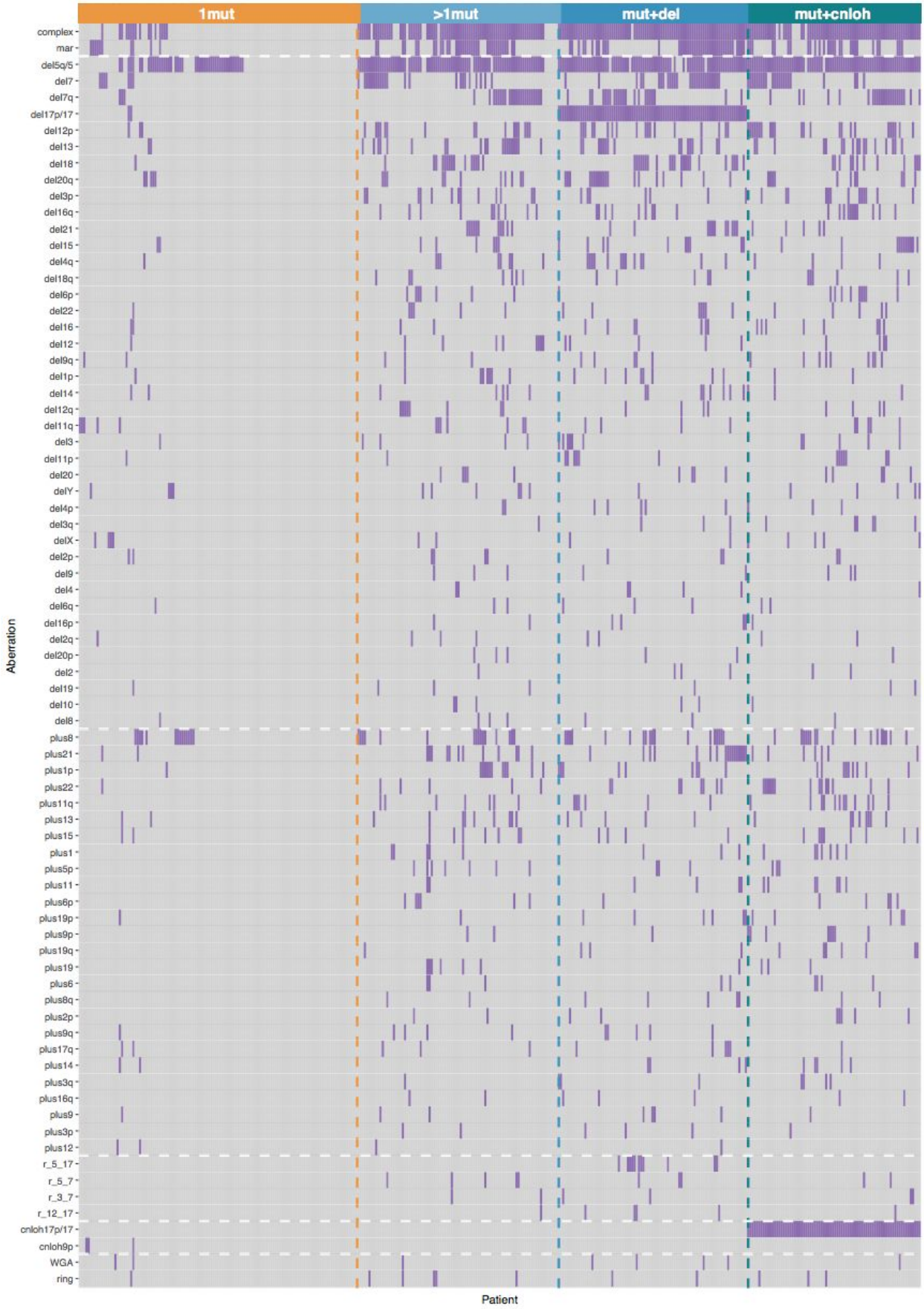

bioRxiv preprint doi: https://doi.org/10.1101/2019.12.19.868844; this version posted December 19, 2019. The copyright holder for this preprint (which was not certified by peer review) is the author/funder, who has granted bioRxiv a license to display the preprint in perpetuity. It is made available under aCC-BY-NC-ND 4.0 International license.

Extended Data Figure 4 | Representation of WHO subtypes and IPSS-R risk groups per *TP53* allelic state. a. Proportion of WHO subtypes per *TP53* state of single gene mutation (1mut) and multiple hits (multi). t-MDS: therapy-related MDS; SLD: single lineage dysplasia; RS: ring sideroblast; MLD: multiple lineage dysplasia; EB: excess blasts; AML-MRC: AML with myelodysplasia-related changes; U: unclassified. Compared to cases with single gene mutation (1mut), multi-hit *TP53* was enriched for t-MDS (21% vs. 8%, OR=2.9, p=0.002 Fisher exact test) and MDS-EB2 (31% vs. 13%, OR=3.1, $p<10^{-4}$). Contrarily, mono-allelic *TP53* (1mut) was enriched for MDS-del5q (15% vs. 2%, OR=8.4, $p<10^{-5}$). **b.** Proportion of IPSS-R risk groups per *TP53* state of single gene mutation (1mut) and multiple hits (multi). Multi-hit *TP53* was strongly enriched for the very-poor category compared to mono-allelic *TP53* state (74% vs. 9%, OR=27, $p<10^{-16}$).

bioRxiv preprint doi: https://doi.org/10.1101/2019.12.19.868844; this version posted December 19, 2019. The copyright holder for this preprint (which was not certified by peer review) is the author/funder, who has granted bioRxiv a license to display the preprint in perpetuity. It is made available under aCC-BY-NC-ND 4.0 International license.

a.

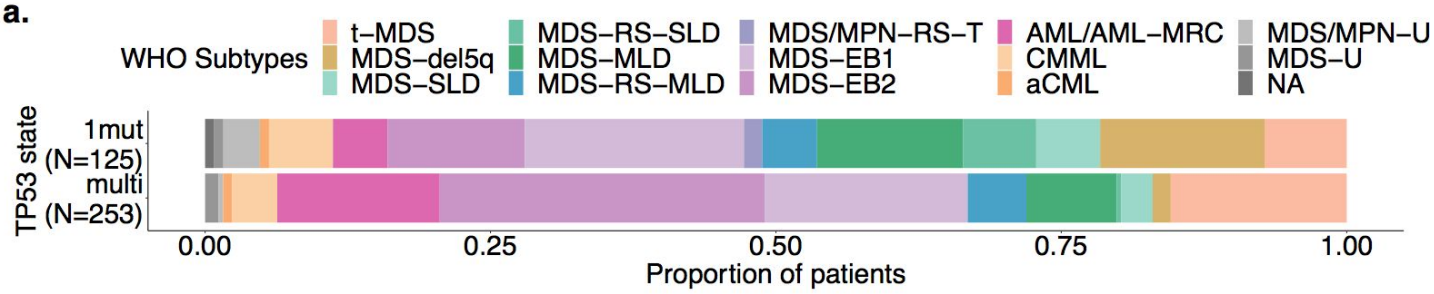

b.

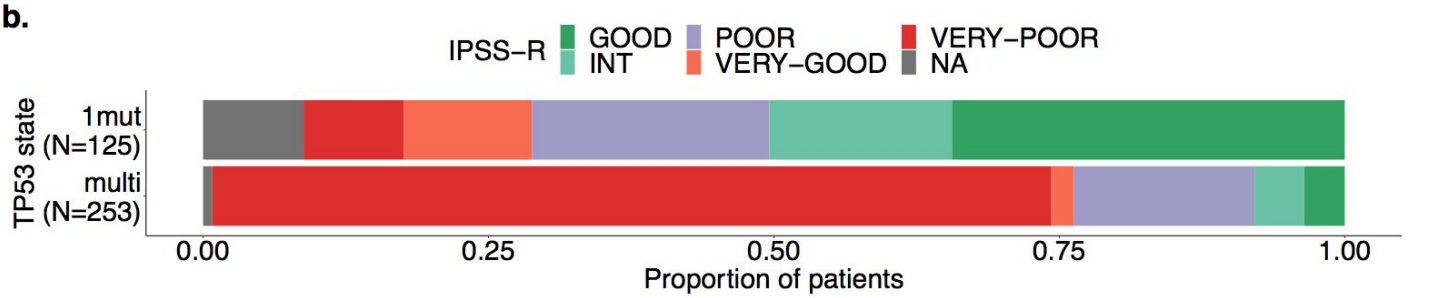

bioRxiv preprint doi: https://doi.org/10.1101/2019.12.19.868844; this version posted December 19, 2019. The copyright holder for this preprint (which was not certified by peer review) is the author/funder, who has granted bioRxiv a license to display the preprint in perpetuity. It is made available under aCC-BY-NC-ND 4.0 International license.

Extended Data Figure 5 | Outcomes across *TP53* subgroups. a. Kaplan-Meier probability estimates of overall survival across *TP53* subgroups of wild-type *TP53* (WT), single *TP53* mutation (1mut), multiple *TP53* mutations (>1mut), *TP53* mutation(s) and deletion (mut+del), *TP53* mutation(s) and copy-neutral loss of heterozygosity (mut+cnloh). **b.** Cumulative incidence of AML transformation (AMLt) across *TP53* subgroups.

bioRxiv preprint doi: https://doi.org/10.1101/2019.12.19.868844; this version posted December 19, 2019. The copyright holder for this preprint (which was not certified by peer review) is the author/funder, who has granted bioRxiv a license to display the preprint in perpetuity. It is made available under aCC-BY-NC-ND 4.0 International license.

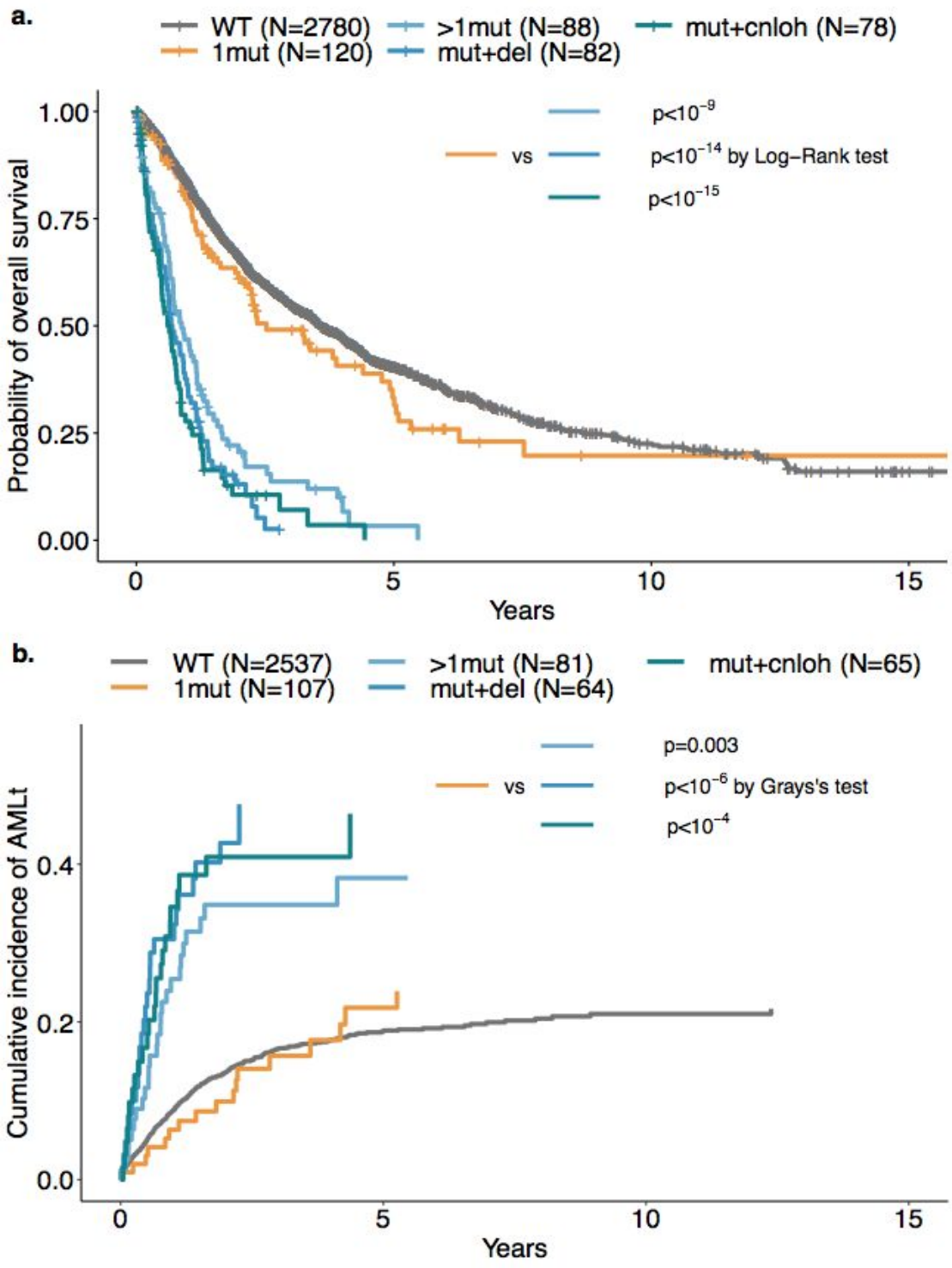

bioRxiv preprint doi: https://doi.org/10.1101/2019.12.19.868844; this version posted December 19, 2019. The copyright holder for this preprint (which was not certified by peer review) is the author/funder, who has granted bioRxiv a license to display the preprint in perpetuity. It is made available under aCC-BY-NC-ND 4.0 International license.

Extended Data Figure 6 | *TP53* allelic state segregates patient outcomes across WHO subtypes and IPSS-R risk groups. a. Kaplan-Meier probability estimates of overall survival across main WHO subtypes per *TP53* state of wild-type *TP53* (WT), single *TP53* mutation (1mut) or multiple *TP53* hits (multi). WHO subtypes MDS-SLD and MDS-MLD are merged together as MDS-SLD/MLD and WHO subtypes MDS-EB1 and MDS-EB2 are merged together as MDS-EB1/EB2. **b.** Kaplan-Meier probability estimates of overall survival across IPSS-R risk groups per *TP53* state of wild-type *TP53* (WT), single *TP53* mutation (1mut) and multiple *TP53* hits (multi). IPSS-R very-good and good risk groups are merged together (leftmost panel), and IPSS-R very-poor and poor risk groups are merged together as well (rightmost panel). Annotated p-values are from the log-rank test.

bioRxiv preprint doi: https://doi.org/10.1101/2019.12.19.868844; this version posted December 19, 2019. The copyright holder for this preprint (which was not certified by peer review) is the author/funder, who has granted bioRxiv a license to display the preprint in perpetuity. It is made available under aCC-BY-NC-ND 4.0 International license.

a.

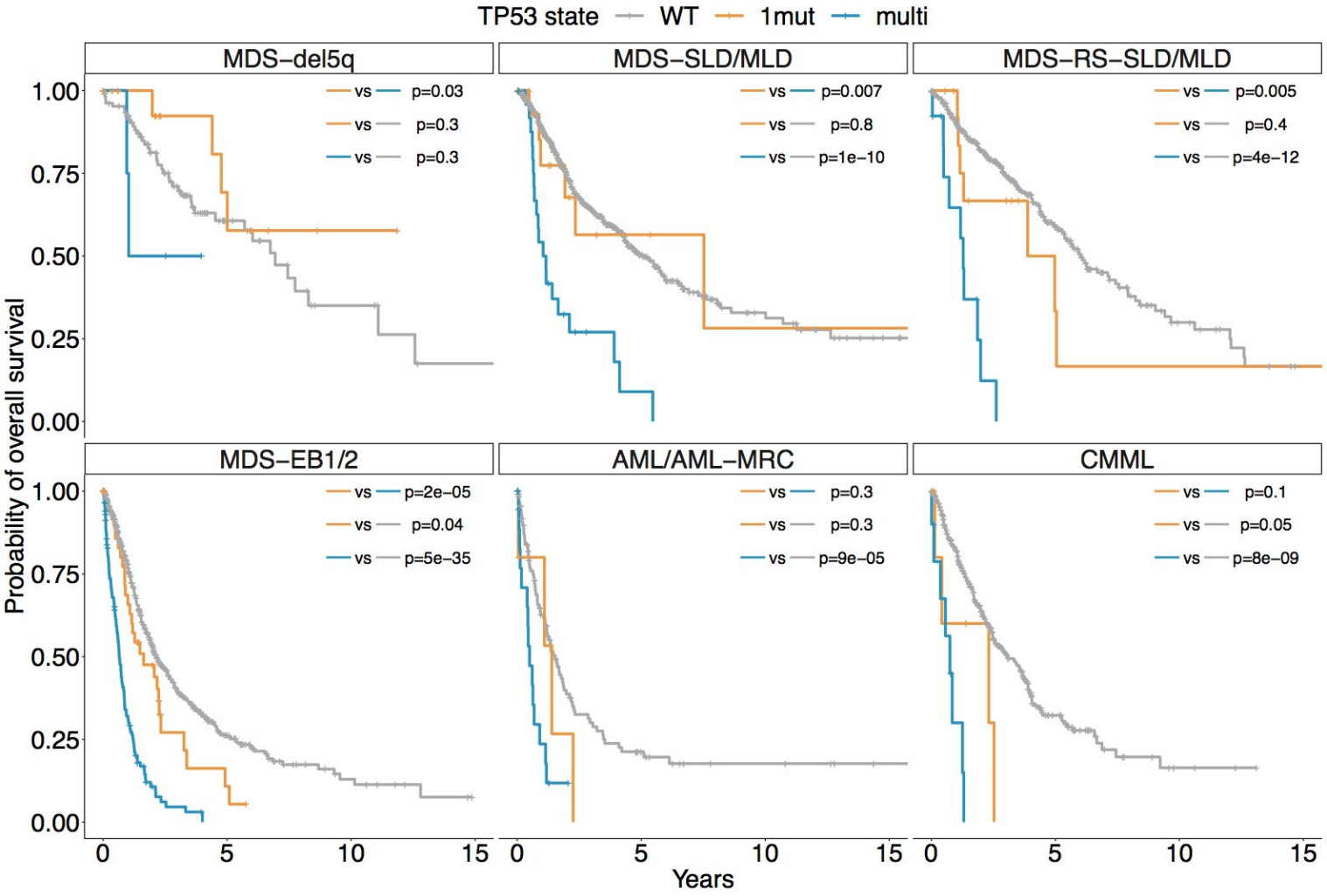

b.

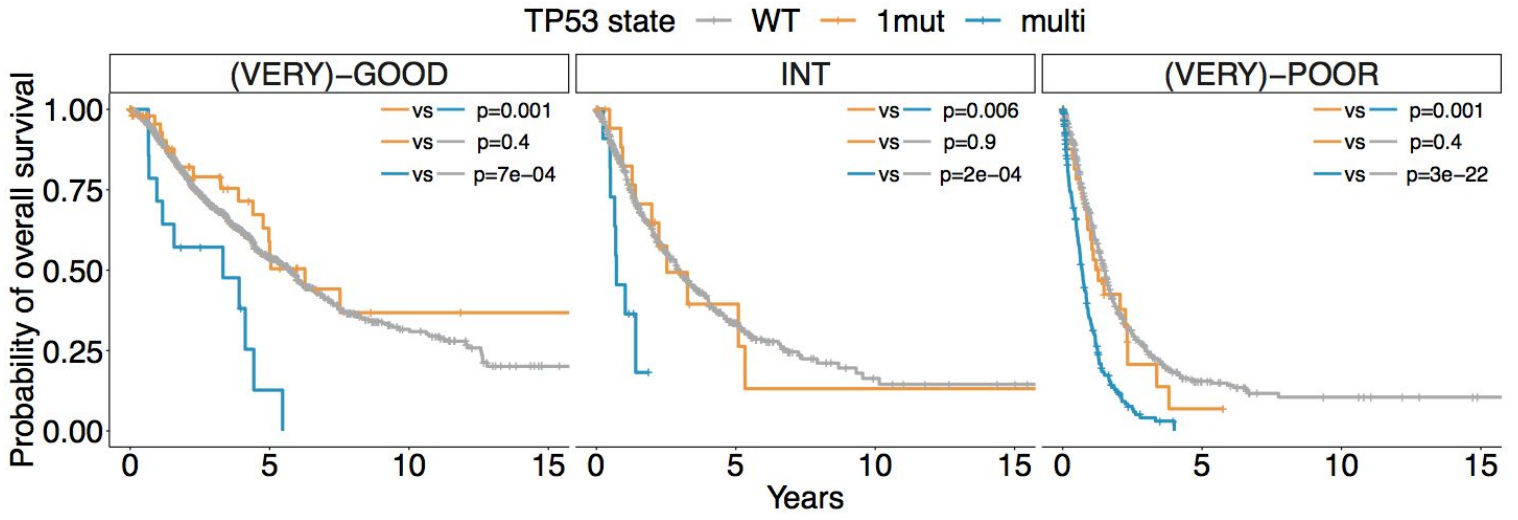

bioRxiv preprint doi: https://doi.org/10.1101/2019.12.19.868844; this version posted December 19, 2019. The copyright holder for this preprint (which was not certified by peer review) is the author/funder, who has granted bioRxiv a license to display the preprint in perpetuity. It is made available under aCC-BY-NC-ND 4.0 International license.

Extended Data Figure 7 | Maintained differences in genome instability levels and outcomes per *TP53* state across mutation types. a. Proportion of mutation types across *TP53* subgroups. Truncated mutations (pink) include frameshift indels, nonsense or nonstop mutations and splice-site variants. Mutations annotated as hotspot (purple) are missense mutations at amino acid positions 273, 248, 220 and 175. Mutations annotated as other-missense (green) are additional missense mutations or inframe indels. Odds ratio and Fisher's test p-values for the proportion of truncated versus non-truncated mutations between the multi-hit *TP53* subgroups and the mono-allelic *TP53* subgroup (1mut) are indicated in the pink parts of the barplot. **b.** Distribution of the number per patient of unique chromosomes other than 17 with aberrations per *TP53* subgroup of single gene mutation (1mut), mutation and deletion (mut+del) and mutation and copy-neutral loss of heterozygosity (mut+cnloh) and across mutation types. Note that 5 patients with both several mutations and deletion or cnloh with ambiguity between the mutation type categories have been excluded for this analysis. ****p<0.0001, Wilcoxon rank-sum test, each compared to the same aberration within the 1mut group. **c.** Kaplan-Meier probability estimates of overall survival per *TP53* subgroup across mutation type. Annotated p-values are from the log-rank test.

bioRxiv preprint doi: https://doi.org/10.1101/2019.12.19.868844; this version posted December 19, 2019. The copyright holder for this preprint (which was not certified by peer review) is the author/funder, who has granted bioRxiv a license to display the preprint in perpetuity. It is made available under aCC-BY-NC-ND 4.0 International license.

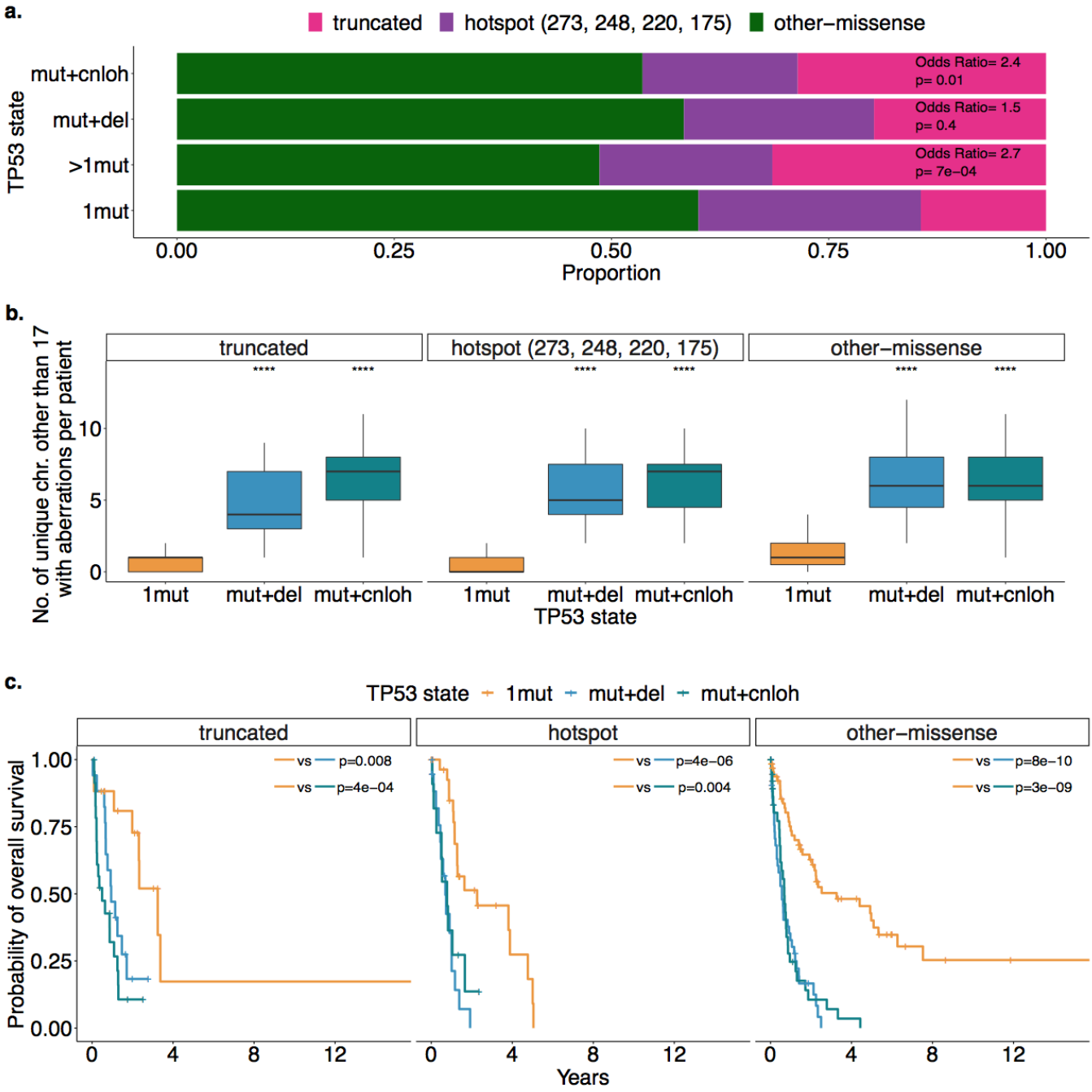

bioRxiv preprint doi: https://doi.org/10.1101/2019.12.19.868844; this version posted December 19, 2019. The copyright holder for this preprint (which was not certified by peer review) is the author/funder, who has granted bioRxiv a license to display the preprint in perpetuity. It is made available under aCC-BY-NC-ND 4.0 International license.

Extended Data Table 1 | Study cohort characteristics. Table describing the baseline characteristics of the study cohort. 1Q: first quartile; 3Q: third quartile; #: AML classification per WHO 2016 and previously RAEB-T cases. $: Median follow-up time is calculated for censored patients.

bioRxiv preprint doi: https://doi.org/10.1101/2019.12.19.868844; this version posted December 19, 2019. The copyright holder for this preprint (which was not certified by peer review) is the author/funder, who has granted bioRxiv a license to display the preprint in perpetuity. It is made available under aCC-BY-NC-ND 4.0 International license.

IWG-MDS cohort (N=3324)		
Characteristic	**No. of cases (%)**	**Median (1Q - 3Q)**
Gender		
Male	2005 (60%)	-
Female	1319 (40%)	-
Age at diagnosis	-	71 (63 - 78)
Missing data	85 (2.6%)	-
Type of MDS		
De-novo	2855 (86%)	-
Therapy-related	229 (7%)	-
Secondary	51 (1%)	-
Missing data	189 (6%)	-
WHO 2016 classification		
MDS		
MDS-del5q	142 (4.3%)	-
MDS-SLD/MLD	914 (27.5%)	-
MDS-RS-SLD/MLD	460 (13.8%)	-
MDS-EB1	451 (13.6%)	-
MDS-EB2	429 (12.9%)	-
MDS-U	92 (2.8%)	-
AML		
AML-MRC	103 (3%)	-
AML[#]	64 (2%)	-
MDS/MPN		
CMML	425 (12.8%)	-
aCML	46 (1.4%)	-
MDS/MPN-U	50 (1.5%)	-
MDS/MPN-RS-T	42 (1.3%)	-
Other	11 (0.3%)	-
Missing data	95 (2.9%)	-
Cytogenetics IPSS-R		
Very-good	125 (3.8%)	-
Good	1992 (59.9%)	-
Int	421 (12.7%)	-
Poor	149 (4.5%)	-
Very-poor	254 (7.6%)	-
Missing data	383 (11.5%)	-
IPSS-R risk group		
Very-good	372 (14.6%)	-
Good	1106 (33.3%)	-
Int	630 (19%)	-
Poor	448 (13.5%)	-
Very-poor	372 (11.2%)	-
Missing data	282 (8.5%)	-
Blood counts		
Hemoglobin (g/dL)	-	9.7 (8.6 - 11.2)
Platelets (10^9/L)	-	123 (65 - 229)
ANC (10^9/L)	-	2 (1 - 3.7)
Bone Marrow Blasts %	-	3 (1 - 8)
Missing data	108 (3.2%)	-
Outcome		
Median follow-up (years)[$]	-	3.44
Missing OS data	152 (4.5%)	-
Missing AML data	163 (4.9%)	-

bioRxiv preprint doi: https://doi.org/10.1101/2019.12.19.868844; this version posted December 19, 2019. The copyright holder for this preprint (which was not certified by peer review) is the author/funder, who has granted bioRxiv a license to display the preprint in perpetuity. It is made available under aCC-BY-NC-ND 4.0 International license.

Extended Data Table 2 | Validation cohort characteristics. Table describing the baseline characteristics of the validation cohort. 1Q: first quartile; 3Q: third quartile; $: Median follow-up time is calculated for censored patients.

bioRxiv preprint doi: https://doi.org/10.1101/2019.12.19.868844; this version posted December 19, 2019. The copyright holder for this preprint (which was not certified by peer review) is the author/funder, who has granted bioRxiv a license to display the preprint in perpetuity. It is made available under aCC-BY-NC-ND 4.0 International license.

Validation cohort (N=1120)		
Characteristic	**No. of cases (%)**	**Median (1Q - 3Q)**
Cohort		
Clinical sequencing	627 (56%)	-
JMPD	314 (28%)	-
JALSG MDS212	179 (16%)	-
Gender		
Male	751 (67%)	-
Female	369 (33%)	-
Age at diagnosis	-	65 (54 - 75)
Missing data	121 (11%)	-
WHO 2016 classification		
MDS		
t-MDS	9 (0.9%)	-
MDS-del5q	7 (0.6%)	-
MDS-SLD	169 (15.1%)	-
MDS-MLD	100 (8.9%)	-
MDS-RS-SLD/MLD	34 (3%)	-
MDS-EB1/2	437 (39%)	-
MDS-U	15 (1.3%)	-
AML		
AML-MRC	121 (10.8%)	-
MDS/MPN		
CMML	43 (3.8%)	-
aCML	4 (0.4%)	-
MDS/MPN-U	6 (0.5%)	-
MDS/MPN-RS-T	4 (0.4%)	-
Missing data	171 (15.3%)	-
IPSS-R risk group		
Very-good	22 (4.2%)	-
Good	60 (11.4%)	-
Int	77 (14.6%)	-
Poor	101 (19.1%)	-
Very-poor	166 (31.4%)	-
Missing data	102 (19.3%)	-
Blood counts		
Hemoglobin (g/dL)	-	8.4 (7.4 - 10.0)
Platelets (10^9/L)	-	76 (39 - 138)
ANC (10^9/L)	-	1.2 (0.5 - 2.4)
Bone Marrow Blasts %	-	6.8 (2 - 15)
Missing data	554 (49%)	-
Outcome		
Median follow-up (years)[$]	-	1.1
Missing OS data	241 (22%)	-

bioRxiv preprint doi: https://doi.org/10.1101/2019.12.19.868844; this version posted December 19, 2019. The copyright holder for this preprint (which was not certified by peer review) is the author/funder, who has granted bioRxiv a license to display the preprint in perpetuity. It is made available under aCC-BY-NC-ND 4.0 International license.

Extended Data Table 3 | Characteristics of treated cohort subsets. Table describing the baseline characteristics of the subset of patients that i) received hypomethylating agent (HMA), ii) received Lenalidomide in the context of del(5q) or iii) underwent hematopoietic stem cell transplantation (HSCT).

bioRxiv preprint doi: https://doi.org/10.1101/2019.12.19.868844; this version posted December 19, 2019. The copyright holder for this preprint (which was not certified by peer review) is the author/funder, who has granted bioRxiv a license to display the preprint in perpetuity. It is made available under aCC-BY-NC-ND 4.0 International license.

Treated cohort subsets			
	HMA cohort (N=656)	**Lenalidomide cohort (N=101)**	**HSCT cohort (N=310)**
Characteristic	**No. of cases (%)**		
TP53 allelic state			
Wild type	511 (78%)	72 (73%)	274 (88%)
Mono-allelic	24 (4%)	12 (12%)	7 (2%)
Multi-hit	121 (18%)	17 (15%)	29 (9%)
TP53 allelic state, with outcome data			
Wild type	497	69	265
Mono-allelic	22	10	7
Multi-hit	119	16	24
Gender			
Male	428 (65%)	35 (35%)	188 (61%)
Female	228 (35%)	66 (65%)	122 (39%)
WHO 2016 classification			
MDS-del5q	4 (0.6%)	50 (50%)	5 (1.6%)
MDS-SLD/MLD	84 (13%)	3 (3%)	59 (19%)
MDS-RS-SLD/MLD	31 (5%)	3 (2%)	21 (6.6%)
MDS-EB1/2	351 (54%)	28 (28%)	144 (46%)
MDS-U	6 (1%)	4 (4%)	7 (2%)
AML/AML-MRC	63 (10%)	6 (7%)	26 (9%)
MDS/MPN	113 (17%)	6 (6%)	45 (14%)
Missing data	4 (0.6%)	1 (0.9%)	3 (0.9%)
Cytogenetics IPSS-R			
Very-good	11 (2%)	-	3 (0.9%)
Good	340 (51%)	63 (63%)	177 (56%)
Int	100 (16%)	6 (6%)	46 (15%)
Poor	58 (9%)	3 (3%)	35 (11%)
Very-poor	111 (17%)	18 (18%)	25 (9%)
Missing data	36 (5%)	11 (11%)	24 (8%)
IPSS-R risk group			
Very-good	19 (3%)	3 (3%)	11 (3%)
Good	95 (14%)	44 (44%)	60 (19%)
Int	151 (23%)	25 (25%)	89 (28%)
Poor	199 (30%)	7 (7%)	87 (28%)
Very-poor	163 (25%)	17 (17%)	50 (17%)
Missing data	29 (4%)	5 (5%)	13 (4%)